npj | science of food

Article

Published in partnership with Beijing Technology and Business University & International Union of Food Science and Technology

https://doi.org/10.1038/s41538-026-00763-1

Mechanism of Morchella polysaccharide in anti-fatigue: the role of the gut microbiota-metabolite axis in mice

Jinyan Liu[1], Jie Li[1], Yixin Li[2], Zihan Gao[2], Le Wang[2], Qian Song[2], Ying Ye[1] ✉ & Jian Liang[2] ✉

This study aims to investigate the anti-fatigue effects of crude Morchella polysaccharide (MP) extracted from the Qinghai-Tibet Plateau region in mice, and to preliminarily explore its potential mechanisms based on the gut microbiota-metabolite axis. Chemical analysis indicates that MP exhibits typical characteristics of crude polysaccharides: it consists of multiple monosaccharides (primarily glucose at 72.33%, along with mannose, galactose, etc) and possesses a broad molecular weight distribution (dispersion index (Mw/Mn) of 30.97). To investigate its material basis, we further isolated and purified the primary water-soluble neutral fraction MP1-1. Structural characterization confirmed MP1-1 as a homogeneous glucan composed solely of glucose units, with a backbone linked via →4)-α-D-Glc*p*-(1 → 4)-type bonds. A negative control group (NC), a positive control group (PC, Rhodiola glycoside,100 mg/kg), and low-, medium-, and high-dose MP groups (50, 100, 200 mg/kg) were established, with continuous gavage for four weeks. Following the final gavage, a weight-bearing swimming test was conducted to record the time to exhaustion and establish a fatigue model. Subsequently, fatigue-related biochemical indicators, gut microbiota composition, and metabolite changes were assessed. The results indicate that MP intervention is significantly associated with an anti-fatigue phenotype. This may occur through regulating the gut microbiota by enriching beneficial bacteria (such as *Lactobacillus* and *Bifidobacterium*) and suppressing harmful bacteria (such as *Desulfovibrio* and *Helicobacter*), thereby reshaping the intestinal microbiome. These alterations were associated with changes in the host's metabolic profile, particularly the upregulation of energy metabolism pathways (e.g., β-alanine metabolism, pentose phosphate pathway, glycerolipid metabolism) and the disruption of inflammation- and oxidative stress-related metabolic pathways. Ultimately, the MP intervention group exhibited increased glycogen reserves, enhanced antioxidant capacity (elevated SOD and GSH-Px; reduced MDA), and reduced systemic inflammation (decreased IL-6 and TNF-α; increased IL-10). Collectively, these effects delayed fatigue onset, promoted recovery, and significantly prolonged swimming duration. In summary, this study suggests that the polysaccharide extract from Morchella elata, native to the Qinghai-Tibet Plateau, may exert anti-fatigue effects by regulating the "gut microbiota-metabolite-host physiological phenotype" network, providing preliminary experimental evidence for its application in the functional food sector.

Fatigue is an inevitable physiological and psychological phenomenon resulting from physical or cognitive activities exceeding a certain intensity or duration[1]. Fatigue leads to impaired memory, reduced work efficiency, and increased safety risks. If prolonged fatigue remains unaddressed, it elevates the risk of cancer and cardiovascular disease mortality[2,3]. Consequently, developing functional foods or drugs with significant anti-fatigue effects has become a research hotspot attracting growing attention. Currently, physical fatigue arises from multiple factors, including neurotransmitter imbalance, accumulation of toxic metabolites, insufficient energy supply, excessive inflammatory responses, gut microbiota dysbiosis, and oxidative stress-

A full list of affiliations appears at the end of the paper. ✉e-mail: yeying08211983@163.com; liangjianws@126.com

induced muscle fatigue[4,5]. Consequently, targeting specific nutrients or supplements based on fatigue mechanisms proves effective in combating fatigue.

Natural products, including bioactive substances derived from plants, animals, and microorganisms, demonstrate multifaceted potential in alleviating fatigue and have become a key focus in the development of functional foods and health supplements. Extensive clinical and preclinical studies indicate that these substances exert anti-fatigue effects through various mechanisms, such as regulating energy metabolism and reducing oxidative stress[6]. For instance, Peng et al. reported that polysaccharides extracted from Bupleurum chinense alleviate fatigue by activating the AMPK/PGC-1αand Nrf2/ARE signaling pathways[7]. Red ginseng extract primarily reduces physical fatigue by enhancing mitochondrial function in skeletal muscle and increasing ATP production[8]. Furthermore, the anti-fatigue effects of garlic polysaccharides are associated with their activation of the AMPK/PGC-1α pathway, reduction of oxidative stress, and regulation of gut microbiota[9]. Among animal-derived active ingredients, pigeon meat hydrolysate (PMH) has been demonstrated to significantly enhance exercise endurance in mice by increasing muscle and liver glycogen stores, alleviating oxidative stress, and regulating energy metabolism[10]. Consequently, natural active ingredients are favored in anti-fatigue research and applications due to their multi-target mechanisms of action and high safety profile.

The Qinghai-Tibet Plateau is the largest and highest plateau on Earth, characterized by unique extreme environmental conditions, including low oxygen levels due to high altitude, intense ultraviolet radiation, low temperatures, and aridity[11,12]. Precisely because of these conditions, this land has shaped and nurtured distinctive food resources such as highland barley, yak products, ribes stenocarpum maxim, and endemic microorganisms[13–16]. To adapt to environmental stressors, these resources typically contain high levels of bioactive compounds like β-glucans, polyphenols, and unsaturated fatty acids. Research has demonstrated their significant potential in energy metabolism, regulating apoptosis and proliferation, and combating fatigue through potent antioxidant, anti-inflammatory, and antibacterial mechanisms, establishing them as a valuable resource pool for developing distinctive functional foods[17–19].

Among the many unique resources of the plateau, Morels (*Morchella spp.*) are a precious edible and medicinal fungus belonging to the Ascomycota phylum. They are named for their uneven caps resembling sheep's stomachs[20,21]. Rich in essential amino acids, polysaccharides, vitamins, minerals, and other nutrients, morels boast exceptionally abundant nutritional components and offer numerous health benefits[22,23]. Notably, morels growing in the extreme environment of the Qinghai-Tibet Plateau may have evolved unique structures and secondary metabolic pathways due to these distinctive conditions, potentially harboring more distinctive bioactive components. Among these active compounds, MP have garnered significant attention for their pronounced antioxidant, lipid-lowering, immunomodulatory, and antitumor effects[24–27]. Research indicates that MP can induce M2 macrophage polarization by upregulating IL-10 and TGF-β expression while downregulating TNF-α and IL-12 expression in mouse peritoneal macrophages, thereby exerting anti-inflammatory and immunomodulatory effects[28]. Furthermore, MP and their selenium-containing derivatives demonstrate potential in anti-fatigue studies, significantly prolonging the exhaustive swimming time in mice and regulating related physiological indicators[29]. The anti-fatigue mechanism of MP may be related to alleviating oxidative stress. MP effectively reduces ROS and MDA levels in PC12 cells while enhancing SOD and GSH activity, thereby protecting PC12 cells from oxidative stress. Concurrently, they inhibit apoptosis by regulating the expression of proteins involved in the PI3K/Akt signaling pathway and mitochondrial apoptosis-related pathways[30].

Research indicates that the biological activity of mushroom polysaccharides is closely related to their monosaccharide composition, molecular weight, and glycosidic bond types[31]. This "structure-activity relationship" is particularly pronounced in fungal polysaccharides. For example, multiple polysaccharide structures have been isolated from Ganoderma lucidum polysaccharides. Among these, Ganoderma lucidum polysaccharide fraction 3 (RF3), featuring a β-glucan backbone, exhibits significant anti-aging effects and immunomodulatory properties[32]. Polysaccharides extracted from termite fungi exhibit anticancer properties. Water-soluble and insoluble β-glucans obtained via hot water extraction significantly stimulate macrophages, thereby demonstrating immunomodulatory characteristics[33]. However, this focus on β-glucans has to some extent obscured the chemical diversity within the fungal polysaccharide realm. In fact, α-configuration glucans also exist in other edible fungi and exhibit unique biological regulatory functions, such as significant anticancer and anti-inflammatory activities[34]. Within the genus Morchella, this structural diversity has been preliminarily confirmed. For instance, a major polysaccharide fraction isolated from *Morchella sextelata* was identified as a glucan with an (1 → 4)-α-D-linked backbone[35]. Our study similarly found that α-glucan constituted the most abundant fraction in MP after isolation and purification.

Although previous studies suggest that morel mushroom polysaccharides (MP) possess anti-fatigue potential, current research on their underlying mechanisms remains insufficient, particularly regarding integrated investigations exploring interactions between gut microbiota and host metabolism. Therefore, this study aims to systematically investigate the anti-fatigue effects of MP on exhausted exercise mice by integrating behavioral studies, physiological and biochemical indicators, histopathology, 16S rRNA gut microbiota sequencing, and non-targeted metabolomics analysis. Notably, to elucidate its material basis, this study systematically isolated and precisely structurally identified the major water-soluble components of MP, confirming the chemical structure of its key active component as α-glucan. Through multi-omics correlation analysis, we aim not only to validate the association between MP and anti-fatigue phenotypes but also to preliminarily reveal the potential link between its specific chemical structure and gut microbiome remodeling, as well as alterations in host metabolic profiles. This will further explore the potential connection between these changes and improvements in key physiological processes such as energy metabolism, oxidative stress, and inflammatory responses. This study provides multi-omics data support for deepening the understanding of MP's anti-fatigue effects, offering a reference for its subsequent research and development.

Results

Basic chemical characteristics of MP

Polysaccharides were extracted from morels originating from the Qinghai-Tibet Plateau. Briefly, hot water extraction was employed, followed by hydrogen peroxide decolorization, the Sevag method for removing free proteins, ethanol precipitation, and freeze-drying to obtain the initial purified product, designated MP, with a polysaccharide content of 72.3%. To clarify the chemical nature of MP used in animal interventions in this study, we first determined its monosaccharide composition and molecular weight distribution. High-performance anion-exchange chromatography (HPAEC) analyzed MP's monosaccharide composition by measuring peak areas and calculating molar ratios. Comparison with a mixed-labeled chromatogram of monosaccharide standards (Fig. 1A) revealed MP to be a heteropolysaccharide composed of multiple monosaccharides. Glucose (Glc) was the predominant monosaccharide component, accounting for 72.33% of the molar ratio, consistent with common reports on Morchella polysaccharides[35]. Additionally, MP contained significant proportions of mannose (Man, 17.92%), galactose (Gal, 8.97%), and trace amounts of glucosamine (GlcN, 0.78%). Therefore, MP constitutes a polysaccharide mixture.

The homogeneity and molecular weight of MP were evaluated using SEC-MALLS-RI (Fig. 1B). The chromatogram revealed an asymmetric broad distribution peak, with a measured weight-average molecular weight (Mw) of 2383.85 kDa, a number-average molecular weight (Mn) of 76.976 kDa, and a polydispersity index (Mw/Mn) of 30.97.

Separation, purification, and preliminary physicochemical characterization of MP

The crude polysaccharide MP was further purified using a DEAE-SEP LIFE FF cellulose column. It was eluted sequentially with ultrapure water and

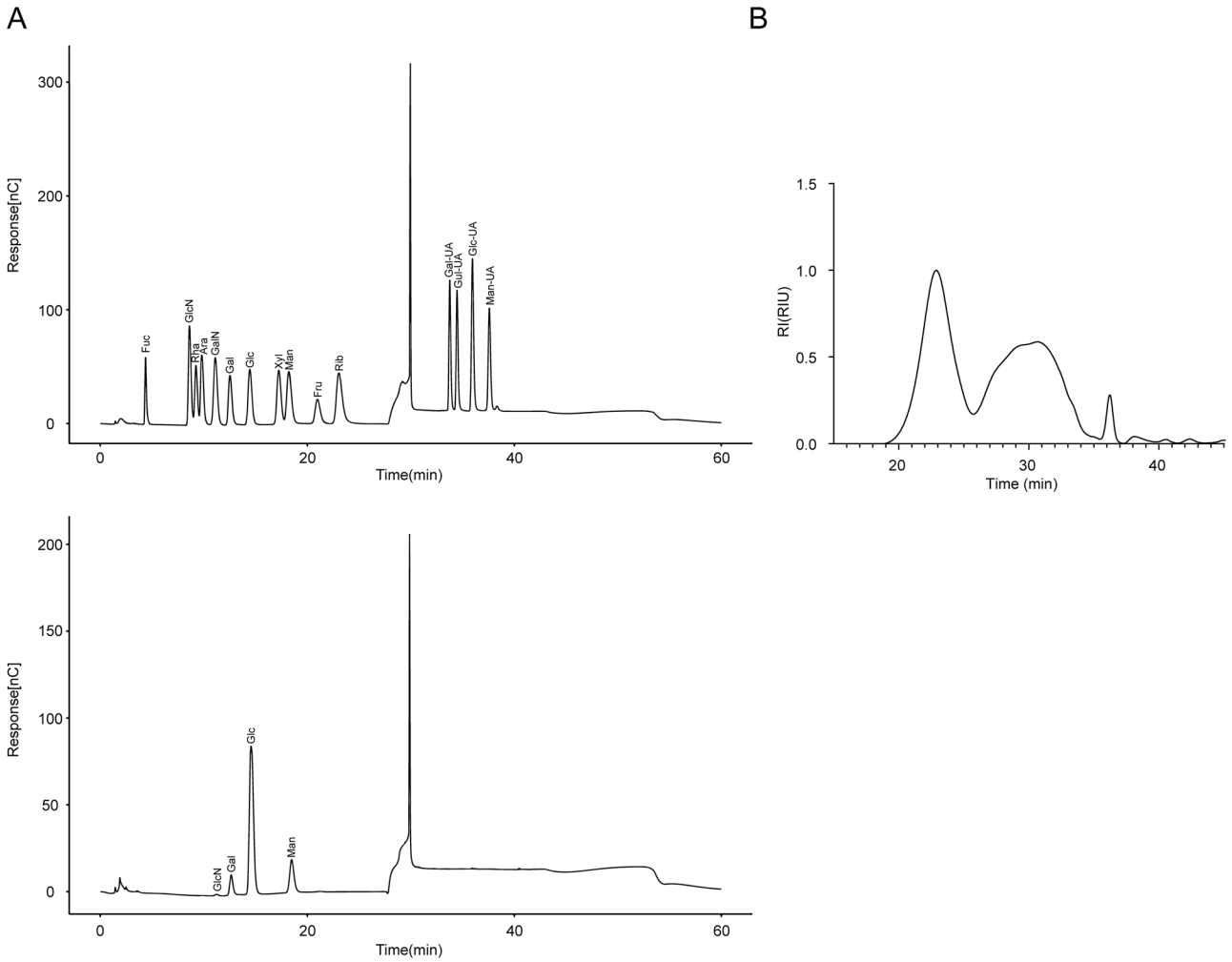

Fig. 1 | Basic Chemical Characteristics of Crude Polysaccharide MP. A Chromatographic analysis results of mixed monosaccharide standard,MP. **B** Molecular Weight Distribution Chromatogram of MP.

stepwise concentrations of NaCl solution (0.1, 0.2, and 0.3 mol/L). The elution curve revealed two major peaks, designated MP1 and MP2 (Fig. 2A). Based on prior studies, the first water-eluted peak (MP1) represented the most abundant neutral polysaccharide fraction and was thus selected for subsequent in-depth investigation.

MP1 was further purified by loading onto a Sephacryl S-400HR gel filtration column, yielding two subfractions (MP1-1 and MP1-2, Fig. 2B). Given MP1-1's superior water solubility compared to the poorly soluble MP1-2, MP1-1 was selected for subsequent structural studies. The recovery rate for MP1-1 loading was 19.2%.

The homogeneity and molecular weight of MP1-1 were evaluated using SEC-MALLS-RI. The symmetrical single peak in the chromatogram (Fig. 2C) confirmed its homogeneity. The weight-average molecular weight (Mw) was determined to be 5.46×10^3 kDa, with a polydispersity index (Mw/Mn) of 1.04. Monosaccharide composition analysis indicated that MP1-1 consisted entirely of glucose (molar percentage: 100.00%), confirming it as a high-purity glucan (Fig. 2D)[7,35].

The Fourier transform infrared spectrum of MP1-1 exhibits characteristic polysaccharide absorption peaks (Fig. 2E). The broad peak at approximately 3410.93 cm^{-1} is attributed to the stretching vibration of -OH groups, while the weak peak around 2928.37 cm^{-1} corresponds to the stretching vibration of C-H bonds. The absorption peak at 1639.95 cm^{-1} is attributed to hydration vibrations of bound water, while the absorption bands at 1411.83 and 1367.64 cm^{-1} are associated with C-H bending vibrations. Multiple strong absorption peaks in the 1000–1200 cm^{-1} range indicate a furanose ring structure. Notably, a weak absorption peak at 849.69 cm^{-1} suggests that the glycosidic bonds in MP1-1 predominantly adopt an α-configuration.

Scanning electron microscopy (SEM) revealed that MP1-1 particles exhibit an irregular lamellar morphology with a relatively smooth and dense surface (Fig. 2F), consistent with the common morphological features of many homogenous polysaccharides.

Fine structure characterization of MP1-1

To precisely determine the glycosidic bond linkages in MP1-1, methylated GC/MS analysis was performed. The results (Table 1) showed that the major glucose residues identified in MP1-1 were t-Glc*p*, 4-Glc*p*, 3,4-Glc*p*, 2,4-Glc*p*, and 4,6-Glc*p*, with proportions of 14.85%, 68.11%, 1.77%, 1.08%, and 14.19%, respectively.

Nuclear magnetic resonance (NMR) spectroscopy further corroborated and refined the above structures. The ^{1}H NMR spectrum (Fig. 3A) exhibited multiple signals in the hetero-hydrogen region (δ 4.3–5.4 ppm), indicating the presence of diverse sugar residues. The chemical shift range for 1H NMR hetero-hydrogen protons was 3.5–5.5 ppm, with α-configuration protons typically exhibiting shifts >4.90 ppm and β-configuration protons typically exhibiting shifts <4.90 ppm[7].

Combining ^{13}C NMR (Fig. 3B) and HSQC (Fig. 3D) with methylation analysis, five major sugar residues were identified by their hetero-signals (Table 2): Residue A (δH/δC 5.34/99.96) corresponds to →4)-α-D-Glc*p*-(1 →; Residue B (4.93/98.73) was α-D-Glc*p*-(1 →; residue B (4.93/98.73) was →4,6)-α-D-Glc*p*-(1 →; residue D (5.16/91.88) was →4)-α-D-Glc*p*; residue E (4.59/95.79) was β-D-Glc*p*-(1 →.

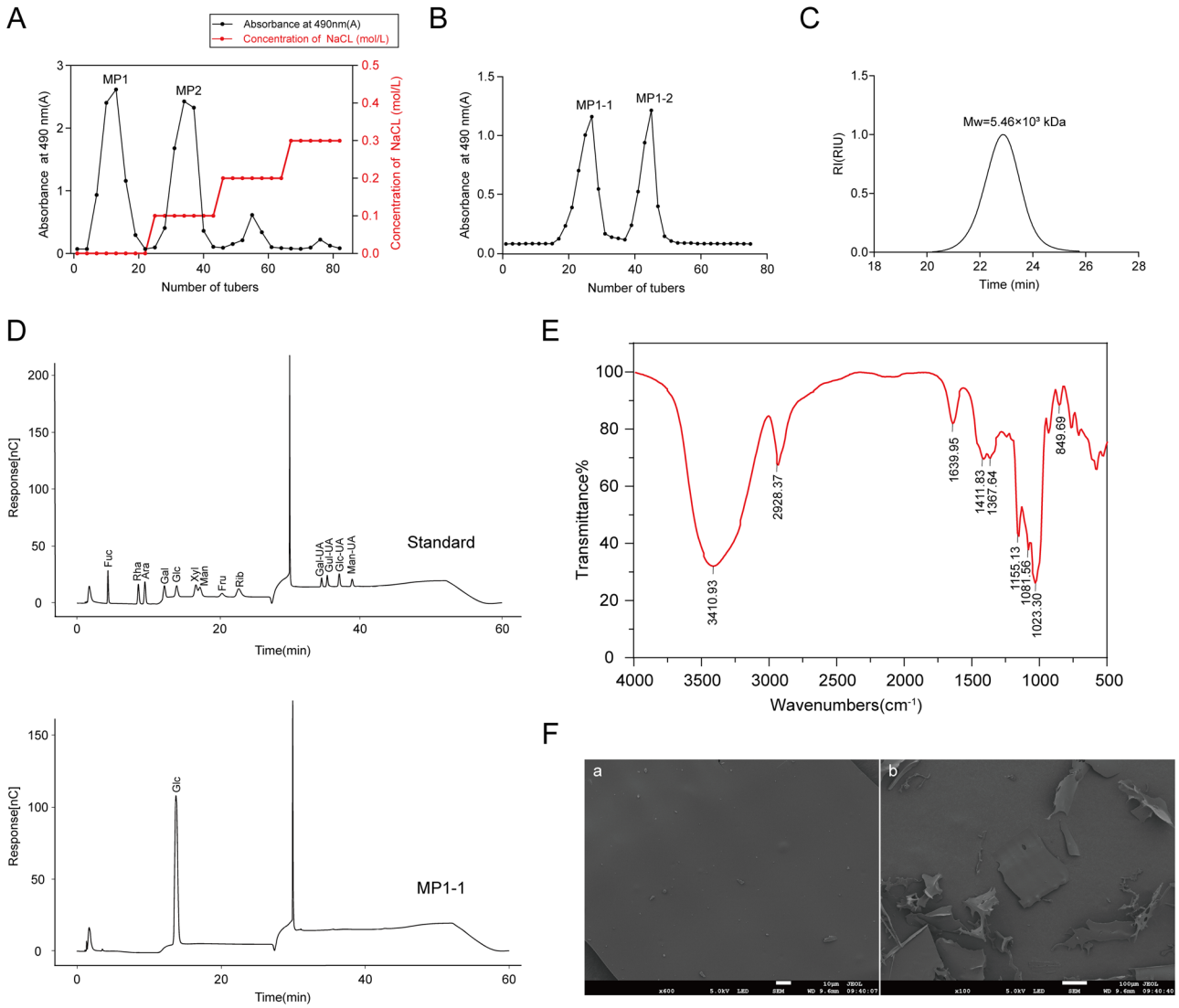

Fig. 2 | Separation, Purification, and Preliminary Structural Characterization of MP. A Elution profile of MP on a DEAE seplife FF column. **B** Elution Curve of Sephacryl S-400HR on MP1. **C** Molecular Weight Distribution Chromatogram of MP1-1. **D** Chromatographic analysis results of mixed monosaccharide standard,MP1-1. **E** Fourier transform infrared (FT-IR)spectra of MP1-1. **F** Scanning electron microscopy of MP1-1(x600,x100).

Table 1 | Methylation analysis of MP1-1

Retention Time(min)	PMAAs	Linkage Pattern	Relative amount(mol%)
9.528	1,5-di-O-acetyl-2,3,4,6-tetra-O-methyl glucitol	t-Glc(*p*)	14.85
14.811	1,4,5-tri-O-acetyl-2,3,6-tri-O-methyl glucitol	4-Glc(*p*)	68.11
17.001	1,3,4,5-tetra-O-acetyl-2,6-di-O-methyl glucitol	3,4-Glc(*p*)	1.77
17.671	1,2,4,5-tetra-O-acetyl-3,6-di-O-methyl glucitol	2,4-Glc(*p*)	1.08
19.115	1,4,5,6-tetra-O-acetyl-2,3-di-O-methyl glucitol	4,6-Glc(*p*)	14.19

Key NOESY spectra (Fig. 3F) reveal spatial connections between sugar residues: H1 of residue A correlates with its own H4 (δ 5.34/3.60) and residue C's H4 (δ 5.34/3.58); H1 of residue B correlates with residue C's H6 (δ 4.93/3.91); and residue C's H1 correlated with residue A's H4 (δ 5.30/3.60). No distinct heteronuclear long-range correlation signals were observed in the HMBC spectrum (Fig. 3E).

Based on the integrated 1D/2D NMR and methylation data, the main chain of MP1-1 is inferred to consist of alternating →4)-α-D-Glc*p*-(1→ and →4,6)-α-D-Glc*p*-(1→ residues. The side chain α-D-Glc*p*-(1→ is attached at the O-6 position on residue C at the branching point. The inferred polysaccharide chain structure is shown in Fig. 3G.

MP had no significant effect on body weight or organ wet weight in mice

Throughout the entire experimental period, the body weights of mice in all groups gradually increased. Compared with the NC group, no significant differences were observed in body weights among mice administered different doses of MP via oral gavage (Fig. 4). This weight gain resulted from normal growth and development, indicating that oral MP

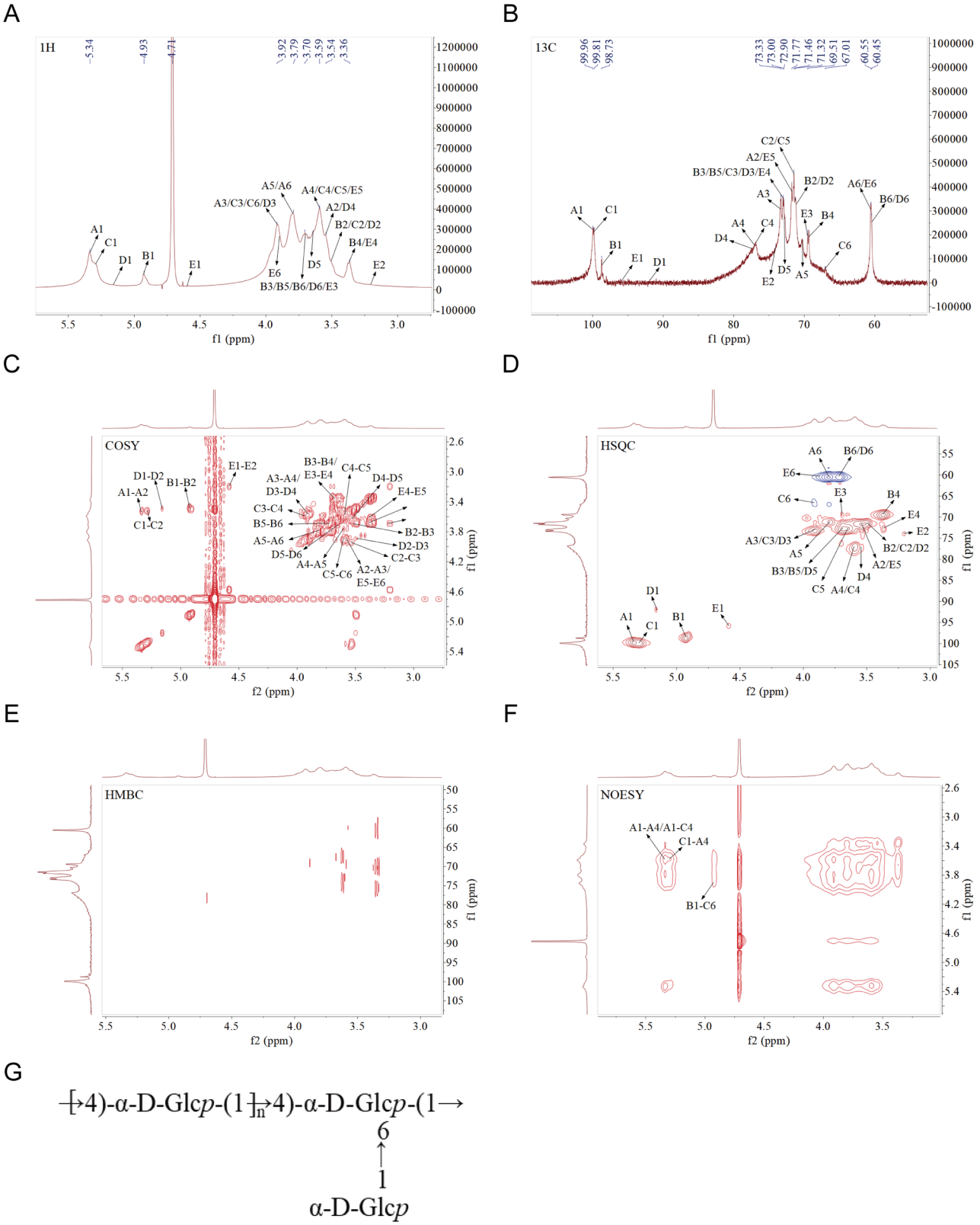

G

Fig. 3 | NMR spectra and proposed structures of MP1-1. A ^{1}H spectrum, **B** ^{13}C spectrum, **C** ^{1}H-^{1}H COSY spectrum. **D** ^{1}H-^{13}C HSQC spectrum. **E** HMBC spectrum. **F** NOESY spectrum. **G** proposed structures of MP1-1.

administration did not significantly promote or inhibit mouse growth. After dissection and weighing of organ wet weights across all groups, statistical analysis revealed no significant differences in organ wet weights between any MP dose group and the NC group (Table 3). This indicates that oral administration of MP at different doses had no discernible effect on mouse organ weights.

Table 2 | ^{1}H and ^{13}C chemical shift assignments of MP1-1

Code	Glycosyl residues		Chemical shifts(ppm)					
			1	2	3	4	5	6
A	→4)-α-D-Glc*p*-(1→	H	5.34	3.55	3.9	3.6	3.79	3.8
		C	99.96	71.77	73.33	77.11	71.19	60.55
B	α-D-Glc*p*-(1→	H	4.93	3.5	3.69	3.37	3.72	3.71
		C	98.73	71.32	72.9	69.35	72.7	60.45
C	→4,6)-α-D-Glc*p*-(1→	H	5.30	3.52	3.93	3.58	3.61	3.91
		C	99.82	71.46	73	76.85	71.52	67.01
D	→4)-α-D-Glc*p*	H	5.16	3.49	3.89	3.54	3.63	3.68
		C	91.88	71.04	72.99	77.39	72.71	60.49
E	β-D-Glc*p*-(1→	H	4.59	3.21	3.7	3.37	3.58	3.88
		C	95.79	73.97	69.51	72.80	71.7	60.61

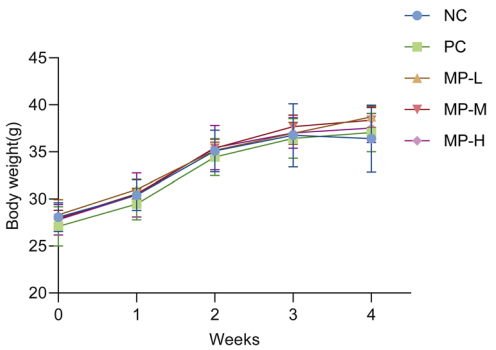

Fig. 4 | Effect of MP on body weight in mice.

Table 3 | Influence of MP on wet weight of mice viscera

Groups	Heart (g)	Liver (g)	Spleen (g)	Kidney (g)
NC	0.18 ± 0.01^{B}	1.47 ± 0.1^{A}	0.1 ± 0.01^{A}	0.49 ± 0.04^{A}
PC	0.19 ± 0.01^{AB}	1.5 ± 0.11^{A}	0.09 ± 0.02^{A}	0.47 ± 0.02^{A}
MP-L	0.2 ± 0.02^{AB}	1.49 ± 0.1^{A}	0.09 ± 0.01^{A}	0.49 ± 0.04^{A}
MP-M	0.21 ± 0.01^{AB}	1.51 ± 0.08^{A}	0.09 ± 0.01^{A}	0.46 ± 0.04^{A}
MP-H	0.2 ± 0.01^{AB}	1.59 ± 0.17^{A}	0.09 ± 0.01^{A}	0.46 ± 0.04^{A}

Each value represents the mean ± standard error ($n = 6$). Different capital letters indicate significant differences between values within a column ($p < 0.05$).

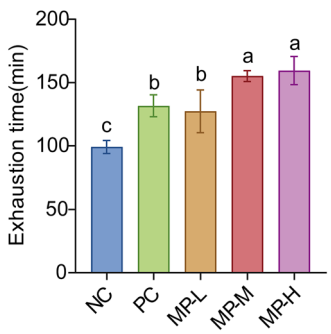

Fig. 5 | Effect of MP on exhausted swimming time in mice. Different lowercase letters indicate significant differences between data ($p < 0.001$).

MP significantly increased exhaustive swimming time in mice

Compared with the NC group, MP intervention significantly prolonged the time to exhaustion in the mouse swim test (Fig. 5) in a dose-dependent manner. Specifically, the MP-L, MP-M, and MP-H groups showed significant increases of 28.4% ($P < 0.001$), 56.5% ($P < 0.0001$), and 60.8% ($P < 0.0001$), respectively. The swimming performance of MP-treated groups was comparable to that of the positive control (PC, Rhodiola glycoside) group.

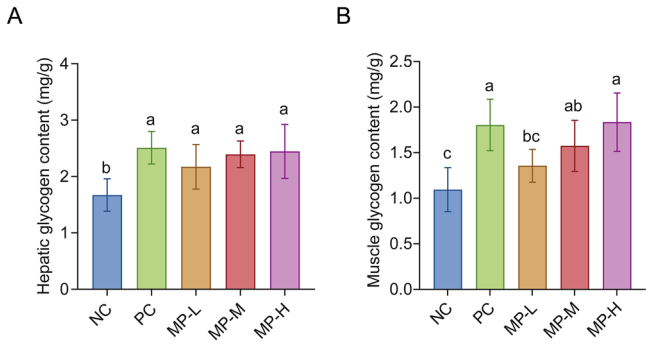

Fig. 6 | Effects of MP on hepatic glycogen and muscle glycogen. A, B Different lowercase letters indicate significant differences between data ($p < 0.01$).

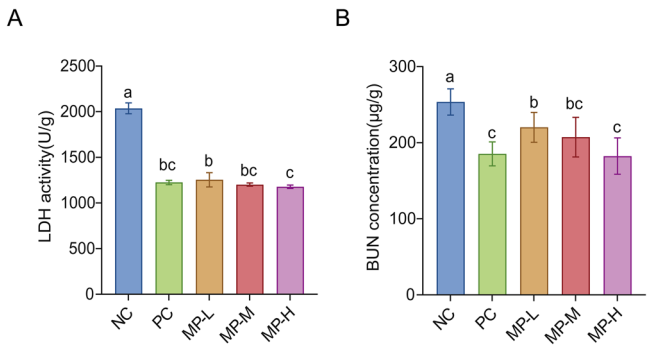

Fig. 7 | Effect of MP on LDH activity and BUN contents in mice. A, B Different lowercase letters indicate significant differences between data ($p < 0.001$).

MP increased the reserves of hepatic glycogen and muscle glycogen in mice

As shown in Figure 6A and B, compared with the NC group, the PC group exhibited significantly increased levels of hepatic glycogen (HG) and muscle glycogen (MG). This finding aligns with literature reports indicating that rhodiola glycosides improve energy metabolism[36]. Compared with the NC group, the HG and MG contents in the MP-L, MP-M, and MP-H groups were significantly increased ($P < 0.01$). The MP-H group achieved glycogen levels comparable to those in the PC group, with no statistically significant difference between the two groups ($P > 0.05$).

MP significantly reduced blood urea nitrogen (BUN) and lactate dehydrogenase (LDH) activity

As shown in Figure 7A and B, compared with the NC group, LDH activity was significantly reduced in all MP dose groups ($P < 0.001$), with the MP-H group exhibiting the greatest reduction. Its activity level was (1177.49 ± 17.08) U/g, representing a 42.20% decrease. Concurrently, BUN levels in all intervention groups were significantly lower than those in the NC group ($P < 0.05$). The MP-H group reduced BUN levels to the lowest extent, with no statistically significant difference compared to the PC group. These findings indicate that MP intervention, particularly at high doses, effectively suppresses LDH release and BUN accumulation induced by exhaustive exercise.

MP improves oxidative stress induced by exhaustive exercise

To evaluate the correlation between MP intervention and oxidative stress status, this study measured tissue levels of malondialdehyde (MDA), total

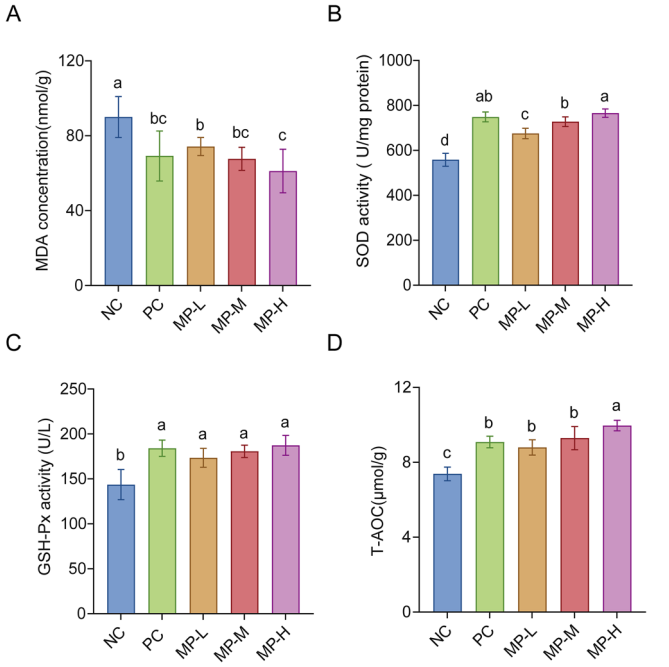

Fig. 8 | Effect of MP on MDA content and antioxidant enzyme activity in hepatic in mice. A–D Different lowercase letters indicate significant differences between data ($p < 0.01$).

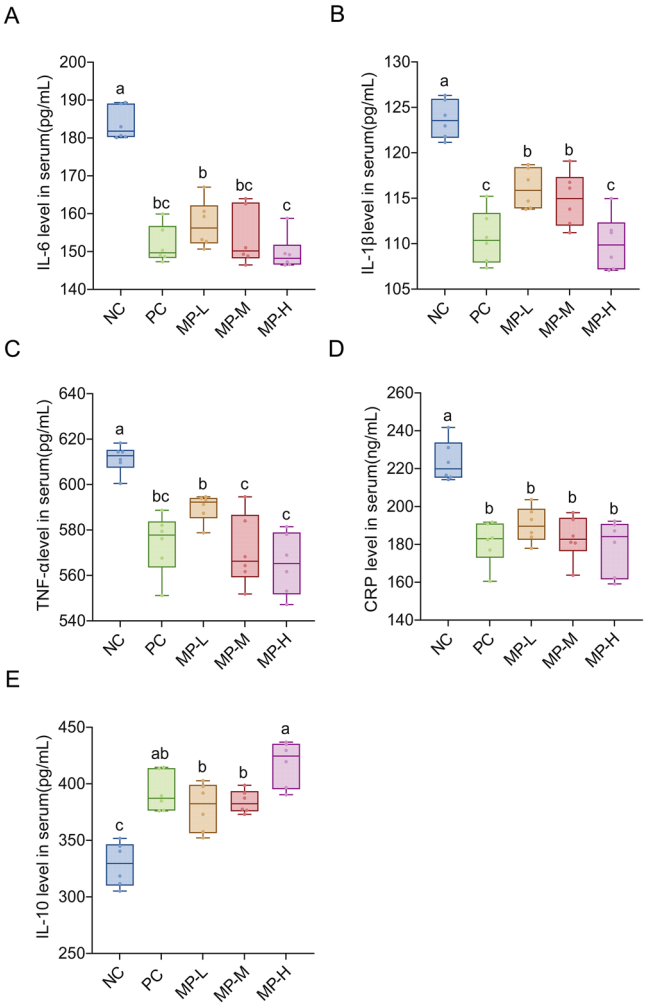

Fig. 9 | Effect of MP on serum cytokine in mice. A–E Different lowercase letters indicate significant differences between data ($p < 0.001$).

antioxidant capacity (T-AOC), and the activity of key antioxidant enzymes superoxide dismutase (SOD) and glutathione peroxidase (GSH-Px). Compared with the NC group, MDA levels were significantly reduced in all MP dose groups ($P < 0.001$) (Fig. 8A). Specifically, MDA levels decreased by 17.52%, 24.79%, and 32.05% in the MP-L, MP-M, and MP-H groups, respectively ($P < 0.05$). Concurrently, antioxidant parameters in MP-treated groups exhibited systematic alterations (Fig. 8B-D): SOD, T-AOC, and GSH-Px activities were significantly elevated compared to the NC group, demonstrating a dose-dependent enhancement trend.

MP can effectively reduce systemic inflammation levels

To assess the correlation between MP intervention and inflammatory status, we measured serum levels of proinflammatory factors (IL-6, IL-1β, TNF-α, CRP) and anti-inflammatory factors (IL-10). As shown in Fig. 9, MP intervention exhibited a dose-dependent association with changes in inflammatory markers. Specifically, compared with the NC group, the MP-H group demonstrated significantly reduced levels of proinflammatory factors, with IL-6, IL-1β, TNF-α, and CRP concentrations decreasing by 18.00%, 11.02%, 7.57%, and 20.12%, respectively ($P < 0.001$). Concurrently, the level of the anti-inflammatory factor IL-10 increased with rising MP dosage, rising by 27.16% in the MP-H group compared to the NC group ($P < 0.001$).

MP exerts a protective effect against exercise-induced multi-organ structural damage

To assess the potential effects of MP intervention on exercise-induced multi-organ tissue states, we performed H&E staining analysis on the heart, liver, skeletal muscle, and kidneys. Histological examination revealed that mice in the NC group exhibited extensive multi-organ structural alterations, including myocardial cell edema, hepatic cell steatosis, disorganized skeletal muscle fiber arrangement, and vacuolar degeneration of renal tubular epithelial cells, accompanied by marked inflammatory cell infiltration (Fig. 10A–D). In contrast, MP intervention attenuated these pathological changes in a dose-dependent manner. The MP-H group exhibited more intact histological structures in major organs, improved cellular morphology, and reduced inflammatory infiltration, with overall histological features comparable to the PC group. These histopathological findings suggest that MP intervention is associated with reduced multi-organ tissue damage induced by exhaustive exercise.

MP improved the gut flora composition of fatigued mice

Our experimental results indicate that α-diversity analysis revealed an upward trend in Shannon, Chao 1, and Ace indices in the MP-H group compared to the NC group. Although these increases did not reach statistical significance, they suggest that MP-H enhanced both the abundance and evenness of the gut microbiota (Table 4 and Fig. 11A–D). Principal coordinate analysis (PCoA) and nonmetric multi-dimensional scaling (NMDS) were employed to analyze the β-diversity of mouse gut microbiota (Fig. 11E). The gut microbiota structures of all MP dosage groups were well separated from the NC group, suggesting that MP supplementation altered the gut microbiota composition in fatigued mice.

To determine the effect of MP on the imbalance of gut flora induced by exercise fatigue, we examined the composition of microorganisms in the mouse cecum. At the phylum level, the dominant phyla in the mouse gut were *Firmicutes* and *Bacteroidetes*, with a combined relative abundance exceeding 70% (Fig. 11I). The relative abundance of *Desulfobacterota* was significantly reduced in the MP dose group compared with NC group ($P < 0.05$). At the genus level, the abundance of *Muribaculaceae* and *Desulfovibrio* gradually decreased in the MP dose group, while that of *Lachnospiraceae* and *Odoribacter* increased (Fig. 11G).

MP intervention also altered the structure of gut microbiota in the mouse cecum (Fig. 11F, H). LEfSe analysis (linear discriminant analysis

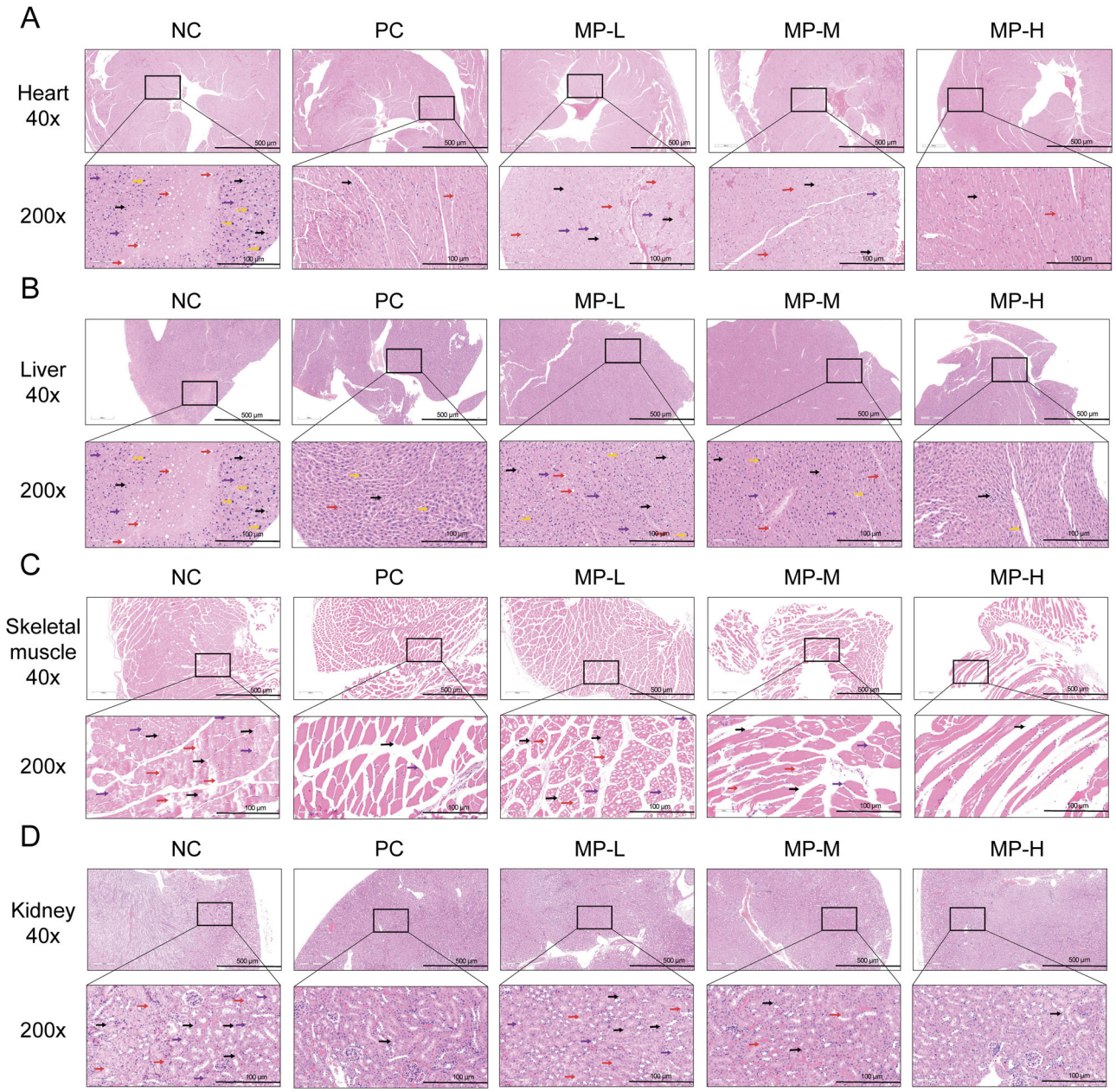

Fig. 10 | Histopathological sections of the heart, liver, skeletal muscle, and kidneys. A Heart.Black arrows: Inflammatory infiltration; Red arrows: cardiac muscle cells; Purple arrows: cell nuclears. **B** Liver. Yellow arrows: Hepatocyte; Red arrows: Lipid degeneration. **C** Skeletal muscle.Red arrows: muscle fiber. **D** Kidney.Red arrows: Renal tubular epithelial cell ; (40x. scale bar = 500μm; 200x. scale bar = 100 μm).

Table 4 | Alpha diversity of samples among different treatment groups

Group	Observed species	Chao 1	ACE	Shannon	Simpson
NC	324.00 ± 29.44	322.70 ± 29.45	322.96 ± 29.28	6.26 ± 0.21	0.95 ± 0.03
PC	335.00 ± 23.64	355.72 ± 21.31	335.05 ± 22.71	6.46 ± 0.07	0.97 ± 0.01
MP-M	330.33 ± 21.59	330.50 ± 20.57	330.15 ± 21.28	6.29 ± 0.62	0.96 ± 0.02
MP-H	335.67 ± 30.89	336.74 ± 29.23	336.06 ± 30.79	6.49 ± 0.14	0.97 ± 0.01

(LDA) > 2, $P < 0.05$) and heatmap analysis revealed increased relative abundance of several key microbial genera in the intestines of MP-H group mice compared to the NC group. These genera included: *Bifidobacterium*, *Lactobacillus*, *Clostridia*, *Bacteroides*, *Colidextribacter*, *Prevotellaceae*, and others. MP intervention reduced the abundance of *Desulfovibrio, Akkermansia*, and *Helicobacter*.

MP helps influence host metabolism to improve energy depletion and metabolic disorders

To elucidate the anti-fatigue effects of MP, untargeted metabolomics was conducted to identify the cecum metabolites in mice. Principal component analysis (PCA) revealed that quality control samples clustered well, indicating reliable data. Additionally, partial overlap was observed between MP-

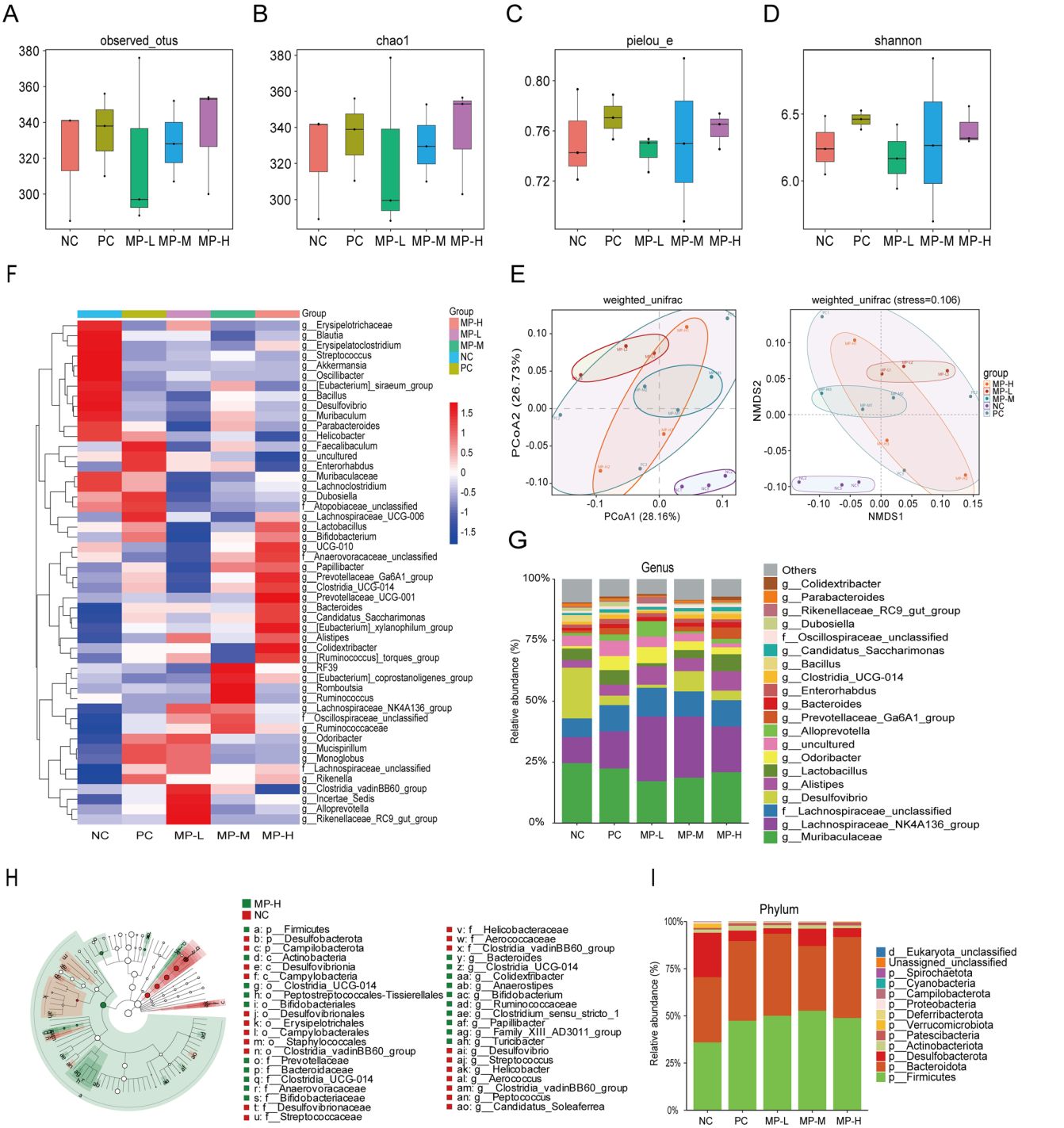

Fig. 11 | Effect of MP on the compositionofthe intestinal flora ofmice. A α-diversity Observed species index. **B** α-diversity Chao 1 index. **C** α-diversity Pielou-e index. **D** α-diversity Shannon index. **E** β-diversity PCoA and NMDS plot. **F** heat map analysis of mice intestinal flora at the genus level. **G** taxonomic distribution of bacteria at the genus level from 16S rRNA sequencing date of cecal contenes. **H** LEfSe analysis. **I** taxonomic distribution of bacteria at the phylum level from 16S rRNA sequencing date of cecal contents. ($n = 3$ for each group).

H and NC group samples, indicating inherent biological variability among individuals (Fig. 12A). Subsequently, orthogonal partial least squares-discriminant analysis (OPLS-DA) further revealed a separation trend in metabolic profiles between MP-H and NC groups (Fig. 12B). Model parameters were $R^2X = 0.193$, $R^2Y = 0.813$, $Q^2 = 0.569$, and the permutation test was significant ($p < 0.05$), indicating differences in metabolic status between the two groups.

According to VIP > 1, P value < 0.05, and fold change(FC) > 1.5 or < 0.67 as screening criteria, a total of 70 differentially expressed metabolites were identified (39 metabolites upregulated, 31 metabolites downregulated) (Fig. 12D). Among these, metabolites with top VIP scores, such as Arachidic Acid, were upregulated in the MP-H group, while 3-Oxocholanic Acid was downregulated (Fig. 12E). Correlation network analysis revealed that these differentially expressed metabolites primarily belonged to major categories including lipids, organic acids, and phenylpropanoids, interacting with each other to form a network (Fig. 12G).

KEGG pathway enrichment analysis revealed that differentially expressed metabolites were significantly enriched in 15 metabolic pathways

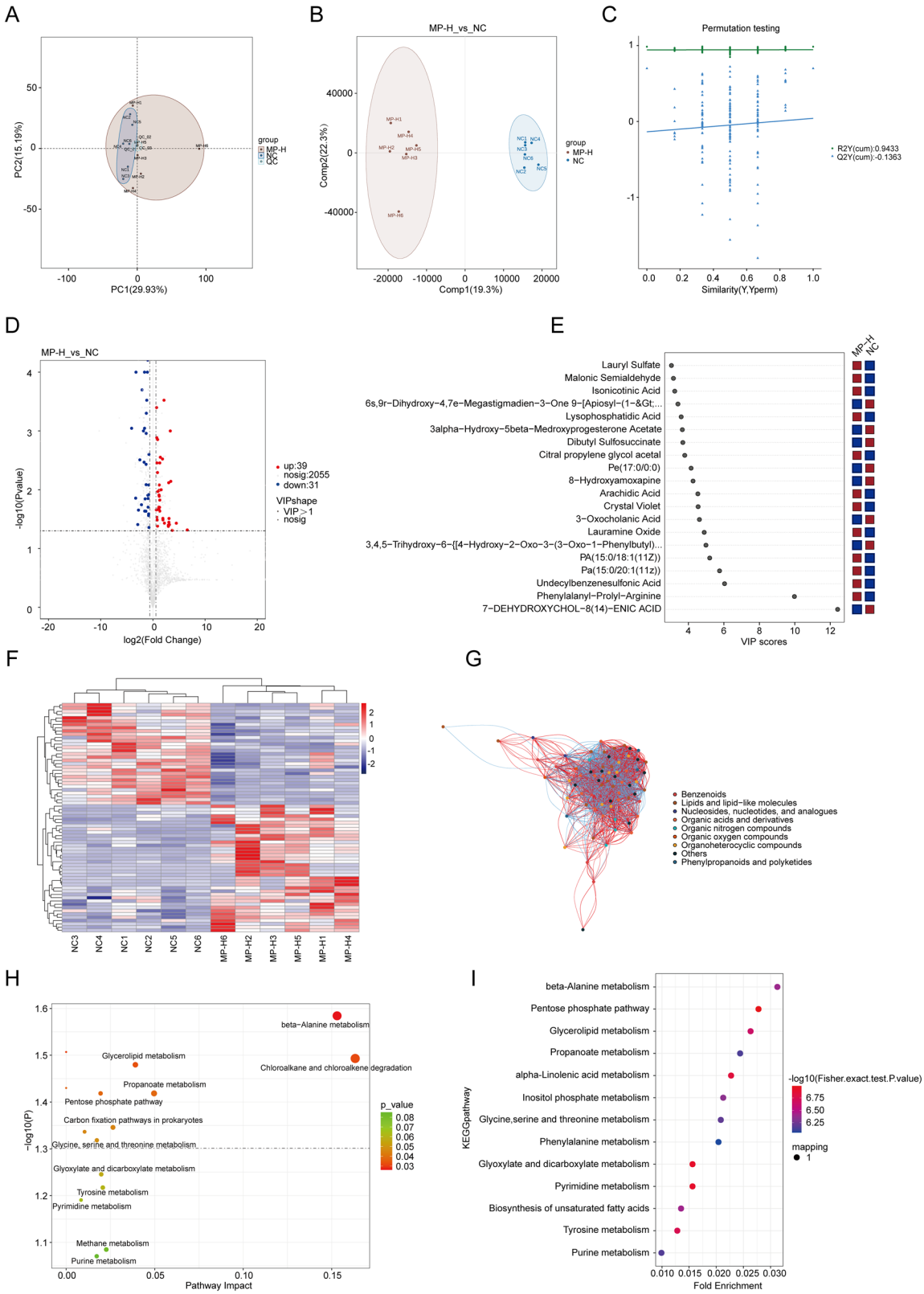

Fig. 12 | Effects of MP on Cecum Metabolome and Key Pathways. A Principal Component Analysis(PCA). **B** Orthogonal partial least squares-discriminant analysis (OPLS-DA) score plot (NC vs. MP-H). **C** OPLS-DA Replacement Test Analysis. **D** Volcano plot showing differentially regulated metabolites between the NC and MP-H groups; red denotes upregulated metabolites, blue represents down-regulated metabolites, and gray indicates non-significant changes. **E** VIP scores show the top 20 metabolites responsible for the data separation. Red modes and blue modes represent up-regulated and down-regulated metabolites in the NC and MP-H groups, respectively. **F** Heat map of differential gene expression. **G** Metabolite-metabolite interaction network. **H** Topological analysis of differential metabolites. **I** Enrichment analysis of different metabolites based on the KEGG database. ($n = 6$ for each group).

(Fig. 12H, I). Among these, beta-Alanine metabolism, Chloroalkane and chloroalkene degradation, Glycerolipid metabolism, Propanoate metabolism, alpha-Linolenic acid metabolism, Inositol phosphate metabolism, pentose phosphate pathway, glycine, serine, and threonine metabolism, and biosynthesis of unsaturated fatty acids were notably disrupted. These findings suggest that MP intervention is associated with extensive reprogramming of the gut metabolic profile, particularly affecting key metabolic pathways related to energy homeostasis and oxidative stress.

Correlation analysis among specific bacterial genera, differential metabolites, and biochemical indices

Spearman correlation analysis can reveal relationships among biochemical markers, fecal metabolites, and gut microbiota. As shown in the heatmap (Fig. S1A), following MP intervention in mice, *Lactobacillus*, *Odoribacter*, and *Clostridia* exhibited positive correlations with antioxidant activity and glycogen reserves, while showing negative correlations with oxidative stress (MDA), BUN, LDH, and inflammatory markers. Conversely, *Desulfovibrio* and *Eubacterium* demonstrated opposite trends. These results are consistent with abundance analysis. As shown in the heatmap (Fig. S1B), following MP intervention in mice, the metabolites 6-Oxopurine, Eicosanoyl-Ea, C4-Homoserine Lactone, Undecylbenzenesulfonic Acid, Lauryl Sulfate, Myristyl Sulfate, Lauramine Oxide, Glyceric Acid, and oxidative stress and inflammatory factors were negatively correlated with antioxidant activity and glycogen reserves. Downregulated metabolites 5-Dihydroxyhept-6-enoic acid, 1,4-Cyclohexanedicarboxylic acid, 2-Carboxy-5-decanolide, 9s-Hydroxy-10-undecenoic acid, 4-Hydroxycoumarin, Isonicotinic Acid, 3and -Oxocholanic Acid were negatively correlated with inflammatory factors, MDA, and BUN, while positively correlated with antioxidant activity and glycogen reserves.

To identify the potential role of microorganisms in MP-induced improvements in specific differential metabolism, spearman correlationanalysis wasperformed between differentially regulated metabolites and the abundant gut microbial taxa identified in mice (Fig. S1C).A mong these, *Desulfovibrio*, *Eubacterium*, and *Muribaculaceae* showed negative correlations with the metabolites 3-Oxocholanic Acid, 1,4-Cyclohexanedicarboxylic Acid, 2-Carboxy-5-Decanolide, 9s-Hydroxy-10-Undecenoic Acid, and 5-Dihydroxyhept-6-Enoic Acid. Conversely, *Lactobacillus*, *Clostridia*, *Acteroides*, and *Odoribacter* showed positive correlations with the metabolites 3-Oxocholanic Acid, 2-Carboxy-5-Decanolide, 9s-Hydroxy-10-Undecenoic Acid, 5-Dihydroxyhept-6-Enoic Acid, and 4-Hydroxycoumarin.

Discussion

Exercise-induced fatigue is a complex physiological phenomenon involving multiple mechanisms, including energy metabolism disorders, oxidative stress, and inflammatory responses[37]. Although the anti-fatigue activity of morel mushroom polysaccharides has been preliminarily reported, the mechanism by which they exert anti-fatigue effects through the "gut microbiota-metabolite axis" remains poorly elucidated. This study integrates behavioral, multi-omics, and structural characterization approaches to explore this mechanism. Notably, the active polysaccharides in edible fungi are primarily β-glucans, with only a few being α-glucans[38]. Among these, β-glucans with a branching degree of 0.2%-0.33% are considered to possess the strongest biological activity[39]. In contrast, α-glucans are less frequently reported in active fungal polysaccharides. Both this study and recent literature indicate that the genus Morchella harbors structurally defined α-glucan resources[35]. This discovery not only confirms the plausible presence of α-glucans in Morchella but also suggests they may exert effects through mechanisms distinct from β-glucans. Recent research isolated three α-glucans from Cynomorium songaricum Rupr. These glucans significantly protected MC3T3-E1 cells from homocysteine-induced oxidative stress damage, manifested as enhanced cell viability, elevated antioxidant enzyme activity, and reduced malondialdehyde and lactate dehydrogenase levels[40].

In this study, we validated the anti-fatigue efficacy of MP by establishing an exhaustive swimming fatigue model. The exhaustive swimming test is widely used in anti-fatigue research[41,42]. Compared with the NC group, the MP-H group significantly prolonged the exhaustive swimming time by 60.8% ($P < 0.0001$) without affecting the mice's baseline physiological status (e.g., body weight), indicating that MP effectively enhances exercise endurance.P revious studies have demonstrated that levels of HG, MG, LDH, and BUN are closely associated with exercise. Exhaustive exercise induces liver damage, leading to a significant increase in serum LDH[43]. LDH, a key enzyme in glycolysis, is commonly used as a marker of muscle damage. Hairtail fish glycoprotein (HGP) exerts anti-fatigue effects by reducing LDH content, inhibiting BLA production, and lowering BUN and CK levels[44]. During muscle fatigue, accumulation of serum urea nitrogen (BUN) metabolites leads to diminished exercise performance[45]. Muscle glycogen serves as a key energy substrate during high-intensity exercise. Its metabolism significantly increases during such exertion but declines markedly within a short timeframe[46]. Acute exercise promotes hepatic glycogenolysis and accelerates gluconeogenesis. When gluconeogenesis and related pathways fail to meet energy demands, AMP-activated protein kinase (AMPK) is activated to enhance lipid oxidation for ATP production —a core mechanism for the liver to ensure systemic energy supply[47]. These findings indicate that acute exercise rapidly depletes energy reserves, activating anaerobic metabolism and increasing lactate accumulation and protein catabolism.In this study, MP significantly increased HG and MG reserves ($P < 0.01$) and markedly reduced LDH and BUN levels ($P < 0.05$), consistent with previous research. This indicates that MP intervention is significantly associated with increased energy reserves (elevated HG and MG) and reduced exercise-induced metabolic disturbances (decreased LDH and BUN). These multifaceted improvements collectively suggest that MP may act through dual pathways—ensuring energy supply and mitigating muscle damage—to delay fatigue onset and enhance exercise endurance.

Exercise-induced muscle damage (EIMD) is caused by primary responses and secondary inflammatory reactions triggered by mechanical stress during exercise, including the production of reactive oxygen species (ROS) and cytokines[48]. When ROS production exceeds the body's natural defense mechanisms, oxidative stress occurs, causing cellular harm through oxidative damage such as lipid peroxidation, DNA damage, and protein misfolding[49]. Among these, attacks on unsaturated fatty acids trigger lipid peroxidation chain reactions, with MDA being one of the primary end products of this process. Its concentration directly reflects the severity of oxidative damage to the body's cells[50–52]. Additionally, elevated LDH levels indicate muscle damage, triggering the release of proinflammatory cytokines, including IL-1β, IL-6, TNF-α, and CRP. These cytokines exacerbate muscle tissue damage and amplify inflammatory responses through oxidative stress pathways[53]. Studies indicate that piperine mitigates microcystin-induced oxidative damage by increasing GSH, SOD, CAT, and GSH-Px levels in mouse livers[54]. Mycelial polysaccharides from Paecilomyces hepiali HN1 (PHMPs) exhibit significant antioxidant activity by elevating serum SOD, GSH-Px, CAT, and T-AOC in mice[55]. Thus, dietary supplements with anti-inflammatory and antioxidant properties may prevent and reduce muscle damage, thereby enhancing exercise endurance[56]. Consistent with this approach, our study revealed that MP intervention was associated with a significant alleviation of oxidative stress in exercise-exhausted mice, manifested by reduced MDA levels and dose-dependent increases in SOD, GSH-Px activity, and T-AOC. At the inflammatory level, MP intervention correlated with decreased serum pro-inflammatory factor levels and elevated anti-inflammatory factor IL-10. These systemic biochemical improvements were corroborated by histopathological observations: skeletal muscle and cardiac tissue in the MP-treated group exhibited milder inflammatory infiltration and structural damage. Collectively, MP intake was closely associated with enhanced antioxidant defense systems, regulated inflammatory responses, and reduced exercise-induced tissue damage—potentially forming a crucial foundation for its exercise endurance-enhancing effects.

In recent years, the role of gut microbiota in alleviating exercise-induced fatigue has garnered significant attention[57–59]. Intense exercise can disrupt gut microbiota balance[60]. Research indicates that high-intensity

interval training (HIIT) increases *Akkermansia* expression levels, whereas no significant difference was observed between the continuous endurance training group and the diabetic group in *Akkermansia* expression levels[61]. The primary reason for the negative correlation between *Akkermansia* abundance and MP intervention in this study likely stems from the longer duration of swimming training in the MP intervention group. Research has shown that low molecular weight walnut protein hydrolysates (LWPs) promote the growth of beneficial microbial populations, such as *Akkermansia*, *Alistipes*, *Eubacterium*, and *Muribaculum*, which are associated with enhanced fatigue resistance[62]. In a 1-methyl-4-phenyl-1,2,3,6-tetrahydropyridine (MPTP)-induced Parkinson's disease (PD) mouse model, significant enrichment of *Desulfobacterota* phylum bacteria was observed in the gut microbiota. These bacteria exacerbate PD progression by driving neuroinflammation and dopaminergic neuron damage[63]. Li FangHang et al. found *Desulfobacterota* exhibits pro-inflammatory properties that activate systemic inflammation[64].

In this study, the MP-H group exhibited a trend toward higher α-diversity indices, suggesting that MP helps maintain a more abundant and balanced gut microbiota. At the phylum level, the composition of the mouse gut microbiota was predominantly dominated by *Firmicutes* and *Bacteroidota*, consistent with previous studies. We observed a dose-dependent reduction in the relative abundance of *Desulfobacterota* by MP, a beneficial shift consistent with the decreased levels of systemic inflammatory markers (e.g., IL-6, TNF-α) detected in the MP intervention group. Furthermore, heatmap analysis revealed that MP intervention was associated with increased abundance of multiple recognized beneficial bacteria (e.g., *Bifidobacterium*, *Lactobacillus*, *Bacteroides*, *Colidextribacter*) and reduced abundance of potentially harmful bacteria (e.g., *Desulfobacter*, *Helicobacter*).

Numerous studies indicate that mushroom polysaccharides play a crucial role in regulating the abundance and composition of gut microbiota, which are closely associated with various diseases[65]. Among these, wild morel mushroom polysaccharides can increase the relative abundance of *Bacteroidetes* while reducing that of *Firmicutes* in the gut[31]. Furthermore, β-glucans increase the abundance of beneficial bacteria such as *Bifidobacterium* and *Lactobacillus*, playing a vital role in maintaining gut microbiota balance[66]. Ganoderma lucidum polysaccharides promote short-chain fatty acid production, repair intestinal barrier damage, and suppress the TLR4/MyD88/NF-κB signaling pathway by regulating the relative abundance of beneficial bacteria like *Lactobacillus* and *Bifidobacterium*, thereby reducing the risk of colitis and carcinogenesis[67].

Increasing the abundance of *Bifidobacterium* and *Lactobacillus* maintains intestinal homeostasis and promotes the production of short-chain fatty acids, which enhance energy metabolism, regulate immune cell function, and alleviate inflammatory responses[68–70]. *Colidextribacter* is an anti-inflammatory probiotic[71], whose abundance negatively correlates with hepatic inflammation and serum total cholesterol (TC) concentration[72]. Elevated GSH-Px activity positively correlates with increased *Colidextribacter* abundance, and higher *Colidextribacter* abundance positively correlates with skeletal muscle antioxidant capacity and glucose metabolism[73]. *Bacteroides*, Gram-negative bacteria, degrade polysaccharides into monosaccharides and short-chain fatty acids, maintaining intestinal barrier integrity, regulating systemic energy metabolism and immune function, and exhibiting anti-inflammatory effects[74–77]. *Helicobacter* is the primary culprit in chronic gastritis, peptic ulcers, and gastric cancer[78]. Based on the above background, we further explored associations between key bacterial genera and host fatigue phenotypes in our study data through Spearman correlation analysis. Results revealed that *Desulfovibrio* and *Eubacterium* abundances positively correlated with pro-inflammatory factors and oxidative stress markers (MDA), while negatively correlating with glycogen reserves. Conversely, *Lactobacillus* and *Odoribacter* abundances positively correlated with anti-inflammatory factors (IL-10), antioxidant enzyme activity, and glycogen levels, and negatively correlated with pro-inflammatory indicators. Thus, the observed gut microbiota remodeling by MP intervention—promoting beneficial genera and suppressing potentially harmful genera—may functionally correlate with reduced host inflammation, alleviated oxidative stress, and improved energy metabolism. This provides a potential mechanistic clue explaining how MP alleviates exercise-induced fatigue through "gut microbiota-host" interactions.

The gut microbiota also plays a crucial role in regulating the body's metabolism. An in vivo mouse study revealed that selenium supplementation induced significant alterations in 31 metabolites in the brains of conventional mice, whereas only 26 metabolites changed in microbiota-depleted mice[79].In this study, untargeted metabolomics analysis revealed that MP intervention significantly remodeled the gut metabolic state of fatigued mice. We identified 70 differentially expressed metabolites, with the upregulation of Arachidic Acid and downregulation of 3-Oxocholanic Acid being the most prominent characteristic changes following MP intervention. This suggests that MP's profound regulation of lipid and bile acid metabolism may be key to its physiological effects. As a long-chain saturated fatty acid, the upregulation of Arachidic Acid directly enhances the body's energy reserves. It can be β-oxidized to provide ample ATP substrates for coping with exercise stress, offering a metabolic basis for the observed increases in glycogen reserves and exercise endurance[80–82]. We observed downregulation of 3-Oxocholanic Acid levels following MP intervention, positively correlated with increased abundance of beneficial bacteria (e.g., *Lactobacillus*) and improved fatigue physiological indicators. This appears to contradict its established role in the literature as a microbiota-derived immunomodulatory molecule[83]. However, this discrepancy represents a critical entry point for understanding the MP system's mechanism of action. We propose that 3-Oxocholanic Acid should not be viewed as an isolated, monofunctional "beneficial" or "harmful" molecule, but rather its changes should be examined within the dynamic network of microbiota-host co-metabolism. First, abnormal bile acid levels (whether elevated or reduced) may indicate metabolic dysfunction[84]. As a metabolite of bile acids, 3-Oxocholanic Acid exhibits cytotoxicity and pro-inflammatory effects at high concentrations. It disrupts mitochondrial function in intestinal epithelial cells, induces oxidative stress and apoptosis, thereby compromising intestinal barrier integrity[85,86]. Consequently, the biological effects of secondary bile acids—including 3-Oxocholanic Acid—are not linearly "more is better." For instance, bacteria such as *Bifidobacterium* can further metabolize 3-oxoLCA into isoallocholic acid (isoalloLCA), which exhibits stronger immunosuppressive activity[87]. Furthermore, in atherosclerosis models, tanshinol borneol ester (DBZ) reduces levels of certain primary and secondary bile acids—such as cholic acid, 7-oxolithocholic acid, hyodeoxycholic acid, and 3-oxocholic acid—toward healthy ranges[88]. Therefore, the downregulation of 3-oxocholanic acid may not represent the end of its functional role but rather signifies the activation of the entire bile acid conversion network and a directed shift in metabolic flux. Its downregulation correlates positively with the abundance of beneficial bacteria (*Lactobacillus*, *Bifidobacterium*), suggesting that MP intervention may promote metabolic pathways converting 3-oxocholanic acid into subsequent, more potent immunomodulatory derivatives. Correlation network analysis indicates that metabolites such as lipids and lipoid molecules, organic acids, and nucleosides serve as key nodes within the MP regulatory network. This reveals that MP's anti-fatigue effects are not mediated by a single metabolite but rather through a complex network of metabolite synergism. Consequently, MP may enhance energy reserves and stabilize cellular structures, thereby providing the body with more sustained energy support and improved resistance to damage.

KEGG pathway enrichment analysis indicates that MP exerts its anti-fatigue effects by optimizing energy supply and enhancing antioxidant defenses through enrichment in key pathways, including β-Alanine metabolism, Glycerolipid metabolism, Propanoate metabolism, Pentose phosphate pathway, and Glycine, serine, and threonine metabolism. β-Alanine metabolism catalyzes the synthesis of carnosine through the combination of β-alanine and histidine via carnosine synthase. Carnosine directly scavenges hydroxyl radicals and singlet oxygen, thereby protecting cell membranes, proteins, and DNA from oxidative damage. This reduces exercise-induced microdamage and inflammation in muscles, accelerating recovery and

delaying fatigue onset[86,89,90]. The pentose phosphate pathway supplies NADPH. Adequate NADPH availability directly supports the efficient operation of glutathione peroxidase (GSH-Px) and the glutathione cycle[91,92]. This further substantiates that MP intervention significantly enhances total antioxidant capacity (T-AOC) while markedly reducing malondialdehyde (MDA) levels.

Our research confirms that MP effectively reduces fatigue induced by strenuous exercise. Furthermore, it was found that MP improves gut microbiota composition by increasing the levels of *Bifidobacterium*, *Lactobacillus*, *Bacteroides*, and *Colidextribacter*, while simultaneously decreasing *Desulfovibrio* and *Helicobacter*. Moreover, MP enhances the body's intrinsic antioxidant capacity, for instance, through mechanisms involving carnosine and the NADPH/glutathione system, while optimizing energy metabolism efficiency via integrated regulation of multiple metabolic pathways. This process confers superior anti-fatigue resilience. The multi-targeted metabolic remodeling mechanism provides robust theoretical support for the development of MP as an effective functional anti-fatigue food. This study has preliminarily elucidated the anti-fatigue mechanism of MP through the "gut microbiota-metabolite axis." Although we focused on MP1-1—the most abundant and water-soluble neutral fraction—and completed its detailed structural characterization, the chemical structures and potential biological activities of other polysaccharide components in MP (such as MP2 and the acidic polysaccharide fraction potentially containing uronic acids) remain unexplored. Therefore, this study retains certain limitations, which simultaneously indicate valuable future directions. Secondly, although we established a robust association between gut microbiota reshaping, metabolic pathway regulation, and the anti-fatigue phenotype through correlation analysis, the causal relationship among these three elements requires more direct experimental evidence for consolidation. We also acknowledge that findings regarding MP's regulation of 3-Oxocholanic Acid, based on non-targeted metabolomics, remain preliminary. This "system reset" hypothesis requires future validation through targeted quantitative bile acid profiling and immune cell functional experiments. The primary findings of this metabolomics analysis are based on uncorrected p-value thresholds; subsequent studies should employ FDR correction for validation. In summary, this work provides preliminary insights into the anti-fatigue effects of Morchella polysaccharides, spanning from overall phenotypes to core component structures, while also revealing its "gut microbiota-metabolite axis" action network. Future research should focus on elucidating the chemical structures of "non-mainstream" components within MP. By designing more causally oriented experiments to dissect the interaction mechanisms among these components and between them and the host microbiota, this work will propel Morchella polysaccharides from a promising crude extract toward becoming a precise functional ingredient or formulation based on well-defined structure-activity relationships.

Methods

Extraction and preparation of MP

Morchella sextelata fruiting bodies were collected from Jianzha County, Qinghai Province, China. They were dried at 45°C to constant weight, pulverized, and sieved through a 60-mesh screen for later use. Crude polysaccharide extraction followed the hot water extraction method with minor modifications. Briefly, an appropriate amount of morel powder was weighed and extracted with ultrapure water at a solid-to-liquid ratio of 1:30 (g/mL) in an 80°C water bath for 2 hours, repeated once. Combined filtrates were concentrated by rotary evaporation, followed by the Sevag method to remove free proteins and multiple decolorizations with hydrogen peroxide. Finally, a fourfold volume of anhydrous ethanol was added to the concentrate for ethanol precipitation. The precipitate was collected, freeze-dried, yielding crude morchella polysaccharide (MP) powder. Total polysaccharide content in MP was determined using the phenol-sulfuric acid method with glucose as the standard, measuring absorbance at 490 nm. Based on the standard curve, the final MP powder contained 72.3% total polysaccharides. The sample was stored at -20°C for subsequent experiments.

Separation and purification of MP

Crude polysaccharide MP was eluted sequentially using distilled water (flow rate 4 mL/min) followed by 0.1 M, 0.2 M, and 0.3 M NaCl solutions on a DEAE Sepharose FF cellulose column (26×400 mm). The elution curve exhibited two major peaks, yielding MP1 and MP2. Based on prior studies, the first water-eluted peak (MP1) represented the most abundant neutral polysaccharide fraction and was thus selected for further investigation. MP1 was separated using a Sephacryl S-400 HR column (26 mm × 1000 mm) and eluted with distilled water at a flow rate of 1.0 mL/min, yielding further purified fractions MP1-1 and MP1-2. Given MP1-1's superior water solubility compared to the poorly soluble MP1-2, MP1-1 was selected for subsequent structural studies. The sample recovery rate for MP1-1 was 19.2%.

Structural characterization of MP1-1

Molecular weight distribution: Dissolve MP1-1 in a 0.1 M $NaNO_3$ aqueous solution containing 0.02% NaN_3 to a concentration of 1 mg/mL, then filter through a 0.45 μm pore size membrane. The weight-average molecular weight (Mw), number-average molecular weight (Mn), and polydispersity index (Mw/Mn) of MP1-1 were determined using high-performance gel permeation chromatography coupled with a differential refractometer and a multi-angle laser light scattering instrument in series.

Monosaccharide Composition Analysis: Place approximately 5 mg of sample into a sealed tube and hydrolyze with 2 M trifluoroacetic acid at 121 °C for 2 hours. Dry the sample under nitrogen, add methanol for washing, evaporate to dryness, and repeat the methanol washing 2-3 times. Residue was redissolved in deionized water, filtered through a 0.22 μm microporous membrane, and analyzed. Sample extracts underwent high-performance anion-exchange chromatography (HPAEC) using a pulse amperometric detector (PAD; Dionex ICS 5000+ system) on a CarboPac PA-20 anion-exchange column (3 × 150 mm; Dionex). Flow rate: 0.5 mL/min; Injection volume: 5 μL; Solvent system A: (deionized water); Solvent system B: (0.1 M NaOH); Solvent system C: (0.1 M NaOH, 0.2 M NaAc); Gradient program: Solvent A:B:C volume ratio at 0 min: 95:5:0; at 26 min: 85:5:10; at 42 min: 85:5:10; at 42.1 min: 60:0:40; at 52 min: 60:40:0; at 52.1 min: 95:5:0; at 60 min: 95:5:0.

Place 10 mg of the MP1-1 sample in the FT-IR spectrometer and record its spectrum in the range of 4000–400 cm^{-1}.

After sample preparation and gold coating, place MP1-1 in the SEM for scanning and photographing at magnifications of 100×, 600×, and 4000×.

The polysaccharide sample was dissolved in dimethyl sulfoxide (DMSO). This solution underwent methylation with chloroform (CH_3I) in a DMSO/sodium hydroxide (NaOH) system. Following methylation, the fully methylated product was hydrolyzed with 2 mol/L trifluoroacetic acid (TFA) at 121°C for 1.5 hours, then reduced with sodium tetraborate ($NaBD_4$), and finally acetylated with anhydrous acetic acid (acetic anhydride) at 100 °C for 2.5 hours. The acetate ester was dissolved in chloroform and analyzed using an Agilent 6890A-5977B gas chromatography-mass spectrometry (GC-MS) system (equipped with an Agilent BPX70 column, specifications: 30 m × 0.25 mm × 0.25 μm, SGE, Australia) with high-purity helium (split ratio 10:1) as carrier gas and an injection volume of 1 μL. The mass spectrometry analysis was conducted with an initial temperature of 140 °C held for 2.0 minutes, followed by a 3°C/min ramp to 230°Cover 3 minutes. The detection mode employed the SCAN mode with a mass range set from 50 to 350 (m/z).

MP1-1 sample was dissolved in 0.5 mL D_2O to a final concentration of 40 mg/mL. 1D-NMR (^{1}H-NMR, ^{13}C-NMR) and 2D-NMR (COSY, NOESY, HMBC, and HSQC) spectra were acquired at 25°C and 600 MHz using a Bruker AVANCE NEO 600 M NMR spectrometer system (Bruker Corporation, Rüdesheim am Main, Germany).

Animals and experimental design

Totally 50 SPF adultmale SPFmice (6–8 weeks; 18–22 g bodyweight) were provided by the Lanzhou Veterinary Research Institute, Chinese Academy of Agricultural Sciences Laboratory Animal Center, and the Certificate of Quality is No. SCXK(Gansu) 2020-0002). The experiments were conducted

following prescribed animal research guidelines. The mice were raised under standard laboratory conditions with a temperature of 22–25 °C, humidity of 50 ± 5%, and a 12 h light/dark cycle. They were provided with a standard diet (product Code: XT101WC-008, Jiangsu Provincial Collaborative Pharmaceutical and Bioengineering Co., Ltd) and water. This animal study was approved by the Qinghai University Science and Technology Ethics Committee (PJ202501-258) and complies with the National Research Council's Guide for the Care and Use of Laboratory Animals.

After one week of adaptive feeding, mice were randomly assigned to five groups of 10 animals each (5 per cage): negative control (NC), positive control (PC, administered 100 mg/kg/day Rhodiola rosea extract orally, selected as the positive control and dosage reference based on its reported efficacy in a similar mouse exercise fatigue model[16]), and low-, medium-, and high-dose MP groups (MP-L, MP-M, MP-H, administered 50 mg/kg, 100 mg/kg, and 200 mg/kg/day, respectively). All oral volumes were fixed at 0.1 mL/(10 g·body weight), administered once daily. During the experiment, mice underwent two adaptive swimming training sessions (10 minutes each) in the first week, with non-swimmers eliminated. The experiment lasted 28 days, during which mice had free access to food and water, with body weight measured every 3 days.

Weight-bearing swimming test

On Day 28, 30 minutes after the final gavage, a lead weight equivalent to 5% of each mouse's body weight was suspended from its tail. The mice were then placed in a standard swimming tank maintained at a constant temperature of (25 ± 1) °C with a water depth of 50 cm to undergo muscle fatigue exercise. Timing commenced with a stopwatch upon immersion. The interval concluded when the mouse submerged to the tank bottom for 8 seconds, recorded as the time to swimming exhaustion.

Biochemical analysis

The liver, muscle, and kidney tissues were processed with 0.9 mL of sterile physiological saline. Zirconia balls were added to assist with grinding. The samples were then placed in a cryogenic grinder and ground at a speed of 11,000×g for 1 min. The supernatant was collected to obtain the tissue homogenate. The levels of HG, MG, MDA, SOD, GSH-Px, T-AOC, LDH, and BUN were determined using respective commercial kits (Beijing Solarbio Science & Technology Co., Ltd).

Biochemical analysis of the blood

The fresh blood was left to stand for 30 minutes at room temperature and centrifuged at 3000 rpm at 4 °C for 15 minutes. The levels of IL-6, IL-10, TNF-α, IL-1,β and CRP were measured using a commercial kit from Shanghai Hepai Biotechnology Co., Ltd.

Histological analysis

The heart, liver, skeletal muscle, and kidney samples were immobilized in 10% neutral-buffered paraformaldehyde. Following fixation, the tissues were subjected to routine histological processing, dehydrated, and embedded in paraffin blocks. Serial sections were cut at a thickness of 4 μm using a rotary microtome (RM2016, Leica). These sections were then stained with hematoxylin and eosin (H&E) according to the manufacturer's protocol (Kit C2103, Baiqian Du Biotech, Wuhan) and coverslipped with neutral resin. Finally, the stained sections were visualized and digitized under a light microscope equipped with a digital imaging system (DS-U3, Nikon, Tokyo, Japan).

Gut microbiota analysis of cecum content

The cecal microbiota was characterized via 16S rDNA amplicon sequencing. On day 28, cecal contents were collected and preserved at -80°C. DNA extraction was performed with a Soil DNA Kit, and the extracted DNA was assessed for quality and concentration using NanoDrop and agarose gel electrophoresis. The V3-V4 hypervariable regions of the 16S rRNA genes were amplified with barcoded primers 338 F/806 R through a PCR procedure comprising initial denaturation, 25 cycles of amplification, and a final extension step. PCR products were then purified utilizing Agencourt AMPure XP beads, involving sequential binding, ethanol wash, and elution. Equimolar pooling of the purified, fluorometer-quantified amplicons was performed to generate the sequencing library, which was subsequently sequenced on the Illumina NovaSeq platform with a PE250 configuration.

Untargeted metabolomics analysis

The obtained cecal content sample (100 mg) was rapidly frozen in liquid nitrogen and ground into a fine powder using a mortar. Subsequently, 100 μL of ice water and 5 ceramic beads were added to the tissue sample, which was homogenized for 60 seconds using a tissue homogenizer. To extract metabolites, 400 μL of methanol/acetonitrile mixture was added to the homogenate. The solution underwent ultrasonication at 4 °C for 30 minutes, followed by centrifugation at 4 °C and 12,000 rpm for 20 minutes. The supernatant was collected, transferred to a clean microcentrifuge tube, freeze-dried, and stored at −20 °C until analysis. Prior to UHPLC-ESI-MS/MS analysis, resuspend samples in 200 μL of 30% acetonitrile and transfer to an injection vial with an insert. Chromatographic separation was performed at 40°C using a Vanquish ultra-high-performance liquid chromatography system equipped with an HSS T3 column, at a flow rate of 0.3 mL/min with a 2 μL injection volume. Both positive and negative ion modes employed a gradient elution system composed of aqueous and acetonitrile phases. High-resolution mass spectrometry data were acquired using a Q Exactive HFX hybrid quadrupole-electrostatic field orbitrap mass spectrometer equipped with a heated electrospray ionization source, operating in full scan-data-dependent secondary scanning mode.

Statistical analysis

Data visualization was performed with GraphPad Prism 9.0 software. For statistical analysis, one-way ANOVA was conducted using IBM SPSS Statistics 25.0 software, followed by Bonferroni post hoc tests for multiple comparisons. A p-value of less than 0.05 was considered statistically significant, and a p-value less than 0.01 was deemed highly significant.

Data availability

The datasets used and/or analyzed in the current study are available from the corresponding author upon reasonable request.

Received: 7 December 2025; Accepted: 10 February 2026;
Published online: 03 March 2026

References

1. Behrens, M. et al. Fatigue and Human Performance: An Updated Framework. *Sports Med.* **53**, 7–31 (2023).
2. Caldwell, J., Caldwell, J., Thompson, L. & Lieberman, H. Fatigue and its management in the workplace. *Neurosci. Biobehav. Rev.* **96**, 272–289 (2019).
3. Knoop, V. et al. Fatigue and the prediction of negative health outcomes: A systematic review with meta-analysis. *Ageing Res. Rev.* **67**, 20 (2021).
4. Ma, X. et al. Mechanisms of Physical Fatigue and its Applications in Nutritional Interventions. *J. Agric. Food Chem.* **69**, 6755–6768 (2021).
5. Si, X. et al. Mechanisms of fatigue and molecular diagnostics: The application of bioactive compounds in fatigue relief research. *Food Biosci.* **68**, 19 (2025).
6. Jeepipalli, S. P. K., Randeni, N., Du, B. & Xu, B. Critical review on anti-fatigue effects of natural dietary products: Present insights and future trends. Food Sci. Hum. Wellness. https://doi.org/10.26599/FSHW.2025.9250626 (2025).
7. Jiang, P. et al. Structure and potential anti-fatigue mechanism of polysaccharides from Bupleurum chinense DC. *Carbohydr. Polym.* **306**, 14 (2023).
8. Zhang, H. et al. Red ginseng extract improves skeletal muscle energy metabolism and mitochondrial function in chronic fatigue mice. *Front. Pharmacol.* **13**, 12 (2022).

9. Li, T. et al. A soluble garlic polysaccharide supplement alleviates fatigue in mice. *npj Sci. Food* **8**, 10 (2024).
10. Zhang, Y. et al. Anti-fatigue effect of pigeon meat hydrolysate on exercise mice and its underlying mechanism: Related to oxidative stress and energy metabolism. *Food Biosci.* **62**, 13 (2024).
11. Bao, Y. et al. The microbial communities and natural fermentation quality of ensiling oat (Avena sativa L) harvest from different elevations on the Qinghai-Tibet Plateau. *Front. Microbiol.* **13**, 11 (2023).
12. Yan, C. et al. Genome of Laudakia sacra Provides New Insights into High-Altitude Adaptation of Ectotherms. *Int. J. Mol. Sci.* **23**, 18 (2022).
13. Zhang, M. et al. Effects of Lactobacillus plantarum on the Fermentation Profile and Microbiological Composition of Wheat Fermented Silage Under the Freezing and Thawing Low Temperatures. *Front. Microbiol.* **12**, 14 (2021).
14. Qin, C., Wang, H., Zhong, J., Ran, H. & Peng, W. miR-129 Regulates Yak Intramuscular Preadipocyte Proliferation and Differentiation through the PI3K/AKT Pathway. *Int. J. Mol. Sci.* **25**, 13 (2024).
15. Hong, Q., Chen, G., Wang, Z., Chen, X. & Kan, J. Effects of different thermal processing methods on bioactive components, phenolic compounds, and antioxidant activities of Qingke (highland hull-less barley). *Food Sci. Hum. Wellness* **12**, 119–129 (2023).
16. Qiao, Y., Ye, Y., Cai, T., Li, S. & Liu, X. Anti-fatigue activity of the polysaccharides isolated from Ribes stenocarpum Maxim. *J. Funct. Food* **89**, 10 (2022).
17. Liu, Z. & Li, B. Epicatechin and β-glucan from highland barley grain modulated glucose metabolism and showed synergistic effect via Akt pathway. *J. Funct. Food* **87**, 12 (2021).
18. Zhang, Y. et al. Integrated Study of Transcriptome-wide m⁶A Methylome Reveals Novel Insights Into the Character and Function of m⁶A Methylation During Yak Adipocyte Differentiation. *Front. Cell. Dev. Biol.* **9**, 15 (2021).
19. Wang, Y. et al. Comparison of Phenols Content and Antioxidant Activity of Fruits from Different Maturity Stages of Ribes stenocarpum Maxim. *Molecules* **23**, 13 (2018).
20. Sunil, C. & Xu, B. Mycochemical profile and health-promoting effects of morel mushroom Morchella esculenta (L) - A review. *Food Res. Int.* **159**, 9 (2022).
21. Du, X. & Yang, Z. Mating Systems in True Morels (Morchella). *Microbiol. Mol. Biol. Rev.* **85**, 23 (2021).
22. Jacinto-Azevedo, B., Valderrama, N., Henríquez, K., Aranda, M. & Aqueveque, P. Nutritional value and biological properties of Chilean wild and commercial edible mushrooms. *Food Chem.* **356**, 8 (2021).
23. Pei, L. et al. Morel (Morchella spp) intake alters gut microbial community and short-chain fatty acid profiles in mice. *Front. Nutr.* **10**, 11 (2023).
24. Tian, J., Zhang, Z., Shang, Y. & Zheng, Y. Extraction, structure and antioxidant activity of the polysaccharides from morels (Morchella spp): A review. *Int. J. Biol. Macromol.* **264**, 15 (2024).
25. Liu, B. et al. Effect of water-soluble polysaccharides from Morchella esculenta on high-fat diet-induced obese mice: changes in gut microbiota and metabolic functions. *Food Funct.* **14**, 5217–5231 (2023).
26. Meng, X. et al. Structural characterization and immunomodulating activities of polysaccharides from a newly collected wild Morchella sextelata. *Int. J. Biol. Macromol.* **129**, 608–614 (2019).
27. Liu, C. et al. Characteristics and antitumor activity of morchella esculenta polysaccharide extracted by pulsed electric field. *Int. J. Mol. Sci.* **17**, 16 (2016).
28. De, G., Das, D., Koschella, A., Ghosh, S. & Pal, C. A new polysaccharide from fruit bodies of Morchella elata: Chemical structure and immunomodulation abilities. *Carbohydr. Res.* **554**, 12 (2025).
29. Zhao W., Wang Meihua, Y. X. Structure characterization and anti-exercise fatigue effect of selenium polysaccharide from Morchella esculenta. *Sci. Technol. Food Ind.* **45**, 110–120 (2024).
30. Chen, X. et al. A polysaccharide from Morchella esculenta mycelia: Structural characterization and protective effect on antioxidant stress on PC12 cells against H2O2-induced oxidative damage. *Int. J. Biol. Macromol.* **298**, 19 (2025).
31. Zhao, J. et al. The Interaction between mushroom polysaccharides and gut microbiota and their effect on human health: a review. *Biol. -Basel* **12**, 29 (2023).
32. Wang, J., Cao, B., Zhao, H. & Feng, J. Emerging Rroles of Ganoderma Lucidum in anti-aging. *Aging Dis.* **8**, 691–707 (2017).
33. Macharia, J. et al. Are chemical compounds in medical mushrooms potent against colorectal cancer carcinogenesis and antimicrobial growth? *Cancer Cell Int.* **22**, 13 (2022).
34. Avni, S. et al. Olive Mill Waste Enhances α-Glucan Content in the Edible Mushroom Pleurotus eryngii. *Int. J. Mol. Sci.* **18**, 11 (2017).
35. Li, F., Jin, Y., Wang, J. & Xu, H. Structure Identification of Two Polysaccharides from Morchella sextelata with Antioxidant Activity. *Foods* **11**, 13 (2022).
36. Qin, N. et al. Effects of salidroside on exercise tolerance of mice under high altitude hypoxia environment. *Zhejiang da xue xue bao*. *J. Zhejiang Univ. Med. Sci.* **51**, 397–404 (2022).
37. Huang, S. et al. Ethanol extract of propolis relieves exercise-induced fatigue via modulating the metabolites and gut microbiota in mice. *Front. Nutr.* **12**, 18 (2025).
38. Wang, G. et al. Prevention and control effects of edible fungi and their active ingredients on obesity: An updated review of research and mechanism. *J. Funct. Food* **107**, 11 (2023).
39. Maity, P. et al. Structural, immunological, and antioxidant studies of β-glucan from edible mushroom Entoloma lividoalbum. *Carbohydr. Polym.* **123**, 350–358 (2015).
40. Li, M. et al. Structural characterization and protective activity of α-glucans derived from Cynomorium songaricum Rupr. against homocysteine-induced oxidative stress in MC3T3-E1 cells. *Int. J. Biol. Macromol.* **310**, 17 (2025).
41. Chen, Y. et al. Anti-fatigue and anti-oxidant effects of curcumin supplementation in exhaustive swimming mice via Nrf2/Keap1 signal pathway. *Curr. Res. Food Sci.* **5**, 1148–1157 (2022).
42. Zhao, L. et al. Moderate highland barley intake affects anti-fatigue capacity in mice via metabolism, anti-oxidative effects and gut microbiota. *Nutrients* **17**, 19 (2025).
43. Yang, J. et al. Sulforaphane inhibits exhaustive exercise-induced liver injury and transcriptome-based mechanism analysis. *Nutrients* **15**, 17 (2023).
44. Lu, X. et al. The Anti-Fatigue Effect of Glycoprotein from Hairtail Fish (Trichiurus lepturus) on BALB/c Mice. *Foods* **12**, 16 (2023).
45. Wong, Y. et al. Enhanced anti-fatigue and exercise performances due to Huang qi polysaccharide supplementation in mice. *Arab. J. Chem.* **17**, 8 (2024).
46. Vigh-Larsen, J., Ortenblad, N., Spriet, L., Overgaard, K. & Mohr, M. Muscle glycogen metabolism and high-intensity exercise performance: a narrative review. *Sports Med.* **51**, 1855–1874 (2021).
47. Hughey, C. et al. Exercise training adaptations in liver glycogen and glycerolipids require hepatic AMP-activated protein kinase in mice. *Am. J. Physiol. -Endocrinol. Metab.* **326**, E14–E28 (2024).
48. Tanabe, Y., Fujii, N. & Suzuki, K. Dietary supplementation for attenuating exercise-induced muscle damage and delayed-onset muscle soreness in humans. *Nutrients* **14**, 19 (2022).
49. Ebrahimi, N. et al. Protective effects of melatonin against physical injuries to testicular tissue: A systematic review and meta-analysis of animal models. *Front. Endocrinol.* **14**, 15 (2023).
50. Jiang, F., Zhou, L., Zhang, C., Jiang, H. & Xu, Z. Malondialdehyde levels in diabetic retinopathy patients: a systematic review and meta-analysis. *Chin. Med. J.* **136**, 1311–1321 (2023).
51. Yang, M., Guo, R., Chen, X., Song, G. & Zhang, F. Advances in the study of regulators of ferroptosis in head and neck squamous cell carcinoma (Review). *Int. J. Mol. Med.* **51**, 11 (2023).

52. Viola, T. et al. Effects of substance use disorder on oxidative and antioxidative stress markers: A systematic review and meta-analysis. *Addict. Biol.* **28**, 14 (2023).
53. Fernández-Lázaro, D. et al. Omega-3 Fatty Acid Supplementation on Post-Exercise Inflammation, Muscle Damage, Oxidative Response, and Sports Performance in Physically Healthy Adults-A Systematic Review of Randomized Controlled Trials. *Nutrients* **16**, 26 (2024).
54. Shabalala, S. et al. The effect of adiponectin in the pathogenesis of non-alcoholic fatty liver disease (NAFLD) and the potential role of polyphenols in the modulation of adiponectin signaling. *Biomed. Pharmacother.* **131**, 17 (2020).
55. Wu, Z. et al. Extraction, characterization and antioxidant activity of mycelial polysaccharides from Paecilomyces hepiali HN1. *Carbohydr. Polym.* **137**, 541–548 (2016).
56. Elejalde, E., Villarán, M. & Alonso, R. Grape polyphenols supplementation for exercise-induced oxidative stress. *J. Int. Soc. Sport Nutr.* **18**, 12 (2021).
57. Zhang, Y. et al. Total minor ginsenosides exert anti-fatigue effects via antioxidant, anti-inflammatory, regulating gut microbiota and serum metabolism. *Life Sci.* **359**, 12 (2024).
58. Sun, Z. et al. Integrated anti-fatigue effects of polysaccharides and small molecules coexisting in water extracts of ginseng: Gut microbiota-mediated mechanisms. *J. Ethnopharmacol.* **337**, 15 (2025).
59. Jing, Y. et al. Structural characterization and anti-fatigue mechanism based on the gut-muscle axis of a polysaccharide from Zingiber officinale. *Int. J. Biol. Macromol.* **283**, 16 (2024).
60. Zhou, J. et al. Diet and physical activity influence the composition of gut microbiota, benefit on Alzheimer's disease. *Food Sci. Hum. Wellness* **13**, 541–555 (2024).
61. Solouki, S., Gorgani-Firuzjaee, S., Jafary, H. & Delfan, M. Efficacy of high-intensity interval and continuous endurance trainings on cecal microbiota metabolites and inflammatory factors in diabetic rats induced by high-fat diet. *PLoS One* **19**, 22 (2024).
62. Huang, S. et al. Identification and Anti-Fatigue Activity of Walnut Protein Hydrolysate. *Nutrients* **17**, 22 (2025).
63. Xu, Z. et al. N-acetyl-L-leucine protects MPTP-treated Parkinson's disease mouse models by suppressing Desulfobacterota via the gut-brain axis. *Brain Res. Bull.* **202**, 10 (2023).
64. Li, F. et al. Physicochemical characteristics and therapeutic mechanisms of Sargassum horneri-derived soluble dietary fiber in cyclophosphamide-induced intestinal damage via gut microbiota and metabolic modulation. *Food Biosci.* **71**, 15 (2025).
65. Mustafa, F. et al. Edible mushrooms as novel myco-therapeutics: effects on lipid level, obesity, and BMI. *J. Fungi* **8**, 21 (2022).
66. Jayachandran, M., Chen, J., Chung, S. & Xu, B. A critical review on the impacts of β-glucans on gut microbiota and human health. *J. Nutr. Biochem.* **61**, 101–110 (2018).
67. Guo, C. et al. Ganoderma lucidum polysaccharide modulates gut microbiota and immune cell function to inhibit inflammation and tumorigenesis in colon. *Carbohydr. Polym.* **267**, 19 (2021).
68. Khan, I. Editorial: Nutrition to support gut health and the microbiome in athletes. *Front. Nutr.* **10**, 4 (2023).
69. Bindels, L. et al. Gut microbiota-derived propionate reduces cancer cell proliferation in the liver. *Br. J. Cancer* **107**, 1337–1344 (2012).
70. Zhao, L. et al. Rubidium salt can effectively relieve the symptoms of DSS-induced ulcerative colitis. *Biomed. Pharmacother.* **181**, 117574 (2024).
71. Li, R. et al. Gut microbiome signatures in the progression of Hepatitis B virus-induced liver disease. *Front. Microbiol.* **13**, 11 (2022).
72. Zhao, H. et al. Sodium alginate prevents non-alcoholic fatty liver disease by modulating the gut-liver axis in high-fat diet-fed rats. *Nutrients* **14**, 14 (2022).
73. Zhang, P. et al. Maternal consumption of L-malic acid enriched diets improves antioxidant capacity and glucose metabolism in offspring by regulating the gut microbiota. *Redox Biol.* **67**, 18 (2023).
74. Ma, W. et al. Immunomodulatory effects of complex probiotics on the immuno-suppressed mice induced by cyclophosphamide. *Front. Microbiol.* **14**, 10 (2023).
75. Zhao, G. et al. Effects of urbanization and lifestyle habits on the intestinal microbiota of adolescents in eastern China. *Front. Microbiol.* **14**, 13 (2023).
76. Tao, R. et al. Ginseng polysaccharides: Potential antitumor agents. *J. Ginseng Res.* **47**, 9–22 (2023).
77. Song, J. et al. Analysis methods for the gut microbiome in neuropsychiatric and neurodegenerative disorders. *Comp. Struct. Biotechnol. J.* **20**, 1097–1110 (2022).
78. Shu, C. et al. Application of biomaterials in the eradication of Helicobacter pylori: A bibliometric analysis and overview. *Front. Microbiol.* **14**, 17 (2023).
79. Wang, X. et al. Gut microbiota: a new perspective for bioavailability of selenium and human health. *npj Sci. Food* **9**, 22 (2025).
80. Gong, A. et al. Acetyl-CoA carboxylase as potential molecular target of dimethyl trisulfide on inhibiting the Aspergillus flavus growth and aflatoxins production. *LWT-Food Sci. Technol.* **198**, 12 (2024).
81. Wang, D., Wang, T., Yang, Y., He, S. & Wang, Y. The Effects of L-Carnitine, Acetyl-L-Carnitine, and Propionyl-L-Carnitine on Body Mass in Type 2 Diabetes Mellitus Patients. *Front. Nutr.* **8**, 7 (2021).
82. Wang, Y. et al. CPT1A-mediated fatty acid oxidation promotes colorectal cancer cell metastasis by inhibiting anoikis (vol 37, pg 6025, 2018). *Oncogene* **44**, 3149–3150 (2025).
83. Leng, L., Zhou, G., Liu, A., Wang, H. & Ni, Y. Lithocholic Acid Species: Metabolism, Signaling Pathways, and Clinical Significance in Enterohepatic Diseases. *Int. J. Mol. Sci.* **26**, 15 (2025).
84. Jiang, Y. et al. Comparative evidence for intrahepatic cholestasis of pregnancy treatment with traditional chinese medicine therapy: a network meta-analysis. *Front. Pharmacol.* **12**, 15 (2021).
85. Chyau, C. et al. Antrodan alleviates high-fat and high-fructose diet-induced fatty liver disease in C57BL/6 Mice Model via AMPK/Sirt1/SREBP-1c/PPARγ Pathway. *Int. J. Mol. Sci.* **21**, 18 (2020).
86. Lancha, A., Painelli, V., Saunders, B. & Artioli, G. Nutritional strategies to modulate intracellular and extracellular buffering capacity during high-intensity exercise. *Sports Med* **45**, S71–S81 (2015).
87. Gavzy, S. et al. Bifidobacterium mechanisms of immune modulation and tolerance. *Gut Microbes* **15**, 23 (2023).
88. Jia, P. et al. The anti-atherosclerotic effect of tanshinol borneol ester using fecal metabolomics based on liquid chromatography-mass spectrometry. *Analyst* **141**, 1112–1120 (2016).
89. Trexler, E. et al. International society of sports nutrition position stand: Beta-Alanine. *J. Int. Soc. Sport Nutr.* **12**, 14 (2015).
90. Oladosu, Y. et al. Drought resistance in rice from conventional to molecular breeding: a review. *Int. J. Mol. Sci.* **20**, 21 (2019).
91. Chen, H. et al. Glucose limitation sensitizes cancer cells to selenite-induced cytotoxicity via SLC7A11-mediated redox collapse. *Cancers* **14**, 17 (2022).
92. Meduri, G. & Chrousos, G. General adaptation in critical illness: glucocorticoid receptor-alpha master regulator of homeostatic corrections. *Front. Endocrinol.* **11**, 28 (2020).

Acknowledgements

This study was funded by the Science and Technology Plan Project of Qinghai Province (Project No. 2023-ZJ-904T). The funder played no role in study design, data collection, analysis and interpretation of data, or the writing of this manuscript.

Author contributions

Jinyan Liu: conceptualization, investigation, data curation, formal analysis, writing—original draft. Jie Li: Writing-review&amp editing, Investigation. Y.L.: Formalanalysis, Visualization. Z.G.L.W., and Q.S.: formal analysis, methodology. Ying Ye (Corresponding Author) and Jian Liang (Corresponding Author): Conceptualization, Funding Acquisition, writing—review and editing.

Competing interests

The authors declare no competing interests.

Additional information

Supplementary information The online version contains supplementary material available at https://doi.org/10.1038/s41538-026-00763-1.

Correspondence and requests for materials should be addressed to Ying Ye or Jian Liang.

[1]College of Agriculture and Animal Husbandry, Qinghai University, Xining, Qinghai, China. [2]State Key Laboratory of Plateau Ecology and Agriculture, Qinghai University, Xining, Qinghai, China. ✉e-mail: yeying08211983@163.com; liangjianws@126.com